Remote Sensing of Environment 183 (2016) 265–281

Contents lists available at ScienceDirect

Remote Sensing of Environment

journal homepage: www.elsevier.com/locate/rse

Magnitude, spatial distribution and uncertainty of forest biomass stocks in Mexico

Pedro Rodríguez-Veiga [a,b,*], Sassan Saatchi [c], Kevin Tansey [a], Heiko Balzter [a,b]

[a] University of Leicester, Centre for Landscape and Climate Research, Dept. of Geography, University Road, Leicester, UK
[b] National Centre for Earth Observation (NCEO), University of Leicester, University Road, Leicester, UK
[c] NASA-Jet Propulsion Laboratory, 4800 Oak Groove Dr., Pasadena, CA, US

ARTICLE INFO

Article history:
Received 25 January 2015
Received in revised form 4 April 2016
Accepted 1 June 2016
Available online 13 June 2016

Keywords:
Forest biomass
Uncertainty
Forest probability
MODIS
ALOS PALSAR
SRTM
Carbon
MaxEnt
REDD+

ABSTRACT

Existing forest biomass stock maps show discrepancies with *in-situ* observations in Mexico. Ground data from the National Forest and Soil Inventory of Mexico (INFyS) were used to calibrate a maximum entropy (MaxEnt) algorithm to generate forest biomass (*AGB*), its associated uncertainty, and forest probability maps. The input predictor layers for the MaxEnt algorithm were extracted from the moderate resolution imaging spectrometer (MODIS) vegetation index (VI) products, ALOS PALSAR L-band dual-polarization backscatter coefficient images, and the Shuttle Radar Topography Mission (SRTM) digital elevation model. A Jackknife analysis of the model accuracy indicated that the ALOS PALSAR layers have the highest relative contribution (50.9%) to the estimation of *AGB*, followed by MODIS-VI (32.9%) and SRTM (16.2%). The forest cover mask derived from the forest probability map showed higher accuracy ($\kappa = 0.83$) than alternative masks derived from ALOS PALSAR ($\kappa = 0.72$–0.78) or MODIS vegetation continuous fields (VCF) with a 10% tree cover threshold ($\kappa = 0.66$). The use of different forest cover masks yielded differences of about 30 million ha in forest cover extent and 0.45 Gt C in total carbon stocks. The *AGB* map showed a root mean square error (RMSE) of 17.3 t C ha^{-1} and $R^2 = 0.31$ when validated at the 250 m pixel scale with inventory plots. The error and accuracy at municipality and state levels were RMSE $= \pm 4.4$ t C ha^{-1}, $R^2 = 0.75$ and RMSE $= \pm 2.1$ t C ha^{-1}, $R^2 = 0.94$ respectively. We estimate the total carbon stored in the aboveground live biomass of forests of Mexico to be 1.69 Gt C $\pm$ 1% (mean carbon density of 21.8 t C ha^{-1}), which agrees with the total carbon estimated by FAO for the FRA 2010 (1.68 Gt C). The new map, derived directly from the biomass estimates of the national inventory, proved to have similar accuracy as existing forest biomass maps of Mexico, but is more representative of the shape of the probability distribution function of *AGB* in the national forest inventory data. Our results suggest that the use of a non-parametric maximum entropy model trained with forest inventory plots, even at the sub-pixel size, can provide accurate spatial maps for national or regional REDD+ applications and MRV systems.

1. Introduction

Forests sequester carbon through photosynthesis and store it primarily as living aboveground biomass of trees (*AGB*). *AGB* is defined as the mass of living organic material for a given area, and approximately 50% of *AGB* is carbon (IPCC, 2003). Because of the slow turnover time of *AGB*, it is a key quantity when estimating terrestrial carbon stocks. In recognition of its importance, biomass has been identified as an essential climate variable (ECV) by the Global Climate Observing System (GCOS) to support the work of the United Nations Framework Convention on Climate Change (UNFCCC) and the Intergovernmental Panel on Climate Change (IPCC) in monitoring climate change.

Deforestation and forest degradation are considered to be the largest source of greenhouse gas emissions in many tropical countries (Gibbs, Brown, Niles, & Foley, 2007). Accurately monitoring and reporting the *AGB* of forests is a requirement of international policies to mitigate climate change through the reduction of greenhouse gas emissions from deforestation and forest degradation, as well as the enhancement of existing forest carbon stocks (REDD+, Reduction of Emissions form Deforestation and Forest Degradation). The implementation of REDD+ includes an element of measurement, reporting and verification (MRV) for which appropriate systems have to be developed at national, sub-national or project levels.

Mexico is actively participating in the United Nations (UN) climate mitigation programmes and is developing a national REDD+ strategy to include actions at project level and jurisdictional level accompanied by an MRV system at national level. Mexico has already developed a dense network of national forest inventory plots to support national

* Corresponding author.
E-mail addresses: pedro.rodriguez@le.ac.uk (P. Rodríguez-Veiga), saatchi@jpl.nasa.gov (S. Saatchi), kjt7@le.ac.uk (K. Tansey), hb91@le.ac.uk (H. Balzter).

http://dx.doi.org/10.1016/j.rse.2016.06.004

forest policies through geographic and statistical information in which the first cycle started in 1961. These plots are also used in the Mexican national greenhouse gas inventory. However, the inventory plots are designed for large-scale statistics on forest carbon stocks and changes.

A transparent and efficient methodology with frequent updates is required for a national MRV system. It is recognised that a combination of remote sensing data and forest inventory data is required for this purpose, since neither data source is able to satisfy the full data requirements for MRV. Remote sensing data allows the production of spatial maps that can improve GHG monitoring at local and national scales, and provide information that can be used for land use planning and management (Gibbs et al., 2007). For example, by mapping forest biomass, deforestation and forest degradation, it is possible to provide estimates of GHG emissions and removals at local and national scales (Houghton, 2005).

In the past decade, several maps of forest structure and *AGB* have been produced at continental and national levels with resolutions from 250 m to 1 km to represent landscape-scale variations in carbon stocks (e.g. Hansen et al., 2003; Blackard et al., 2008; Lefsky, 2010; Baccini et al., 2012; Baccini, Laporte, Goetz, Sun, & Dong, 2008; Saatchi, Harris, et al., 2011b, Simard, Pinto, Fisher, & Baccini, 2011, Santoro et al., 2011; Thurner et al., 2014). In addition, regional maps at finer spatial resolutions (around 30 m) are available for specific areas (e.g. Hansen et al., 2013; Cartus et al., 2014; Avitabile, Baccini, Friedl, & Schmullius, 2012, Asner et al., 2012; Hame, Rauste, et al., 2013; Hame, Kilpi, et al., 2013). Some of these approaches are limited by the absence of well-distributed *in-situ* sample sites at the scale of the used remote sensing data (Houghton, Hall, & Goetz, 2009), and to some extent by the limited sensitivity of the selected satellite sensors to *AGB* (Patenaude, Milne, & Dawson, 2005).

Passive optical sensors can differentiate vegetation from other surfaces based on the selective absorption of electromagnetic radiation by the chlorophyll-*a* and *b* systems in plants. For the AVHRR and Landsat satellite series, several decades of data are now available from archives. The main shortcoming of these sensors is that visible light cannot penetrate clouds, and passive sensors can only operate during day-time, leading to reduced availability of cloud-free images. Due to their orbital characteristics, there is a trade-off between pixel resolution and higher revisit frequency. Medium resolution (30 m) optical sensors such as those on the Landsat satellites have a 16-day revisit time, which makes it challenging to obtain cloud-free observations over large areas. New products such as the Landsat WELD (Roy et al., 2010) are able to generate monthly, seasonal and annual top-of-atmosphere (TOA) radiance composites at 30 m resolution globally. However, even the annual composites still have gaps in very cloudy areas of the world. The few cloud-free observations acquired over those areas are subject to the time of acquisition in relation to the seasonal phenological cycle. Coarser resolution (250 m) optical sensors such as MODIS have a 24 h revisit time and therefore more opportunities to image under cloud-free conditions than Landsat. In addition, the estimation of *AGB* from optical imagery is limited by the saturation of the signal at low *AGB* (Gibbs et al., 2007).

As active sensors, synthetic aperture radar (SAR) sensors are independent of solar illumination, and can collect imagery during day and night. Microwave radiation also penetrates through haze, clouds and smoke. The radar backscatter (the amount of scattered microwave radiation received by the sensor) is related to *AGB* as the electromagnetic waves interact with scattering elements like leaves, branches and stems. The sensitivity of the SAR backscatter to *AGB* depends on the radar wavelength (Le Toan et al., 2004), with shorter wavelengths being sensitive to smaller canopy elements (X- and C-band), and longer wavelengths (L- and P-band) being sensitive to branches and stems. Longer wavelengths are theoretically more suitable for estimation of *AGB* as tree branches and stems comprise the highest fraction of *AGB* in forests. The sensitivity of L-band SAR backscatter (the longest wavelength available from spaceborne SAR at present) usually saturates between 100 t ha^{-1} and 150 t ha^{-1} (Wagner et al., 2003; Mitchard et al., 2009). Approaches that combine different types of imagery can circumvent the saturation problem and exploit the specific strengths of each sensor over large areas (e.g. Saatchi, Harris, et al., 2011b, Thurner et al., 2014).

Forest map products should not only include forest parameters such as *AGB* but also provide information about their uncertainties. Estimation of the uncertainty at the pixel scale requires a method of error propagation and needs to consider measurement error, allometric error, sampling error, and prediction error. Forest is not a well-defined semantic concept (Wadsworth et al., 2008), hence a certain degree of vagueness in the definition of forest as a land cover type is intrinsic to any forest map, whether it is explicitly described or not. Fuzzy set theory is most commonly used to tackle these issues in spatial data by providing pixel-scale information on the degree of class memberships. Given a specific definition of forest, the degree of forest class membership of each pixel provides a measure of the uncertainty whether the pixel is a forest.

It is important to differentiate between forest area and forest cover. *Forest area* is purely based on land use and includes temporally unstocked areas that are intended for use as forest, while *forest cover* only includes actual forest vegetation, independently of the land use. Forest cover can be estimated from remote sensing data, while forest area needs additional land use information. The forest definition also plays a key role. Sexton et al. (2015) demonstrated the effect of using different forest definitions to generate forest masks from remote sensing data, estimating the discrepancies in global forest extent among eight commonly used satellite products to be up to 13% of the global forest cover. Just within the tropics, the discrepancies between the satellite products lead to a variation in the magnitude of estimated carbon stocks of 45.2 Gt C with a value of approximately US$1 trillion (Sexton et al., 2015).

The Mexican Land Use and Vegetation map (LUV) developed by the Mexican National Institute for Statistics and Geography (INEGI) uses a combination of visual interpretation of optical imagery and field verification to create a land use and vegetation class vector layer at a scale of 1:250,000 (125 m spatial resolution) over the whole Mexican territory (INEGI, 2009). The dataset describes types of forest in Mexico based on several characteristics such as species composition, soils, elevation and climate (INEGI, 2014a) instead of standard biophysical parameters such as minimum canopy cover or canopy height which can be observed in remote sensing imagery. The FAO defines forest as "*Land spanning more than 0.5 hectares with trees higher than 5 meters and a canopy cover of more than 10 percent, or trees able to reach these thresholds in situ*" (FAO, 2012). However, FAO's forest definition also includes temporally unstocked areas. Forest cover maps using the FAO definition while ignoring temporally unstocked areas can be produced from optical and SAR sensors, and are often used in vegetation studies.

MODIS vegetation continuous fields (VCF) and the ALOS PALSAR Kyoto and Carbon Initiative forest/non-forest (K&C-FNF) map are examples of widely used forest cover products based on a similar FAO forest definition but generated from only optical or SAR imagery, respectively (Saatchi, Harris, et al., 2011b, Thiel, Thiel, & Schmullius, 2009, Shimada et al., 2011; Shimada et al., 2014; Hame et al., 2013). MODIS VCF provides annual, global, sub-pixel-scale data of percent tree cover (Hansen et al., 2003) at 250 m spatial resolution. This percent tree cover product is defined as the amount of skylight obstructed by tree canopies equal to or greater than 5 m in height (Hansen et al., 2003). Percent tree cover thresholds above 10%, in accordance with the FAO forest definition, are commonly used to create binary forest/non-forest maps (Saatchi, Harris, et al., 2011b). The VCF percent tree cover definition is slightly different from FAO's canopy cover definition as VCF is based on light penetration through the canopy, while FAO's canopy cover definition is based on crown vertical projection over the ground regardless of light penetration.

The ALOS PALSAR Kyoto & Carbon (K&C) Initiative is an international programme led by the Japan Aerospace Exploration Agency (JAXA)

whose main products are annual forest/non-forest cover maps for the years 2007 to 2010 and 2015 with resolutions from 25 m to 100 m. These products estimate the forest cover using a simple decision tree that is based on a threshold of the horizontal-transmit vertical receive (HV) polarized L-band radar backscatter coefficient (Shimada et al., 2011; Shimada et al., 2014). This threshold is optimized for large regions (e.g. North America, Africa, the Amazon). Forests are defined in this product as areas where the cover of woody vegetation exceeded 10% (Shimada et al., 2014).

The forest maps from MODIS and ALOS PALSAR have different characteristics due to the specific properties of each sensor. For example, using VCF as a forest mask could lead to an erroneous forest extent because the percent tree cover in sparsely vegetated areas tends to be overestimated by VCF (Sexton et al., 2013; Montesano et al., 2009). The PALSAR L-band radar backscatter for crops or settlements can be similar to backscatter from forests and lead to a systematic misclassification of non-forest pixels as forest. Also, forests and woodlands with low biomass, some plantations and high biomass mangroves are often classified as non-forest by the K&C-FNF, as the signal from these cover types is lower than the backscatter threshold for the 'forest' class (Shimada et al., 2014). Estimates of forest cover at continental level by the K&C-FNF differ by −15% to 42% from the Landsat percent tree cover (PTC) product for different continents (Shimada et al., 2014; Hansen et al., 2013). The forest cover estimation from the K&C-FNF is 10.4% lower than the Landsat PTC in North America (Shimada et al., 2014). As a result, a forest *AGB* map using these forest masks would contain an unaccounted element of uncertainty and lead to potentially biased estimations of carbon stocks. How the differences in forest cover estimation affect the estimation of carbon stocks at national and regional levels has not been studied yet.

A study of *AGB* stocks in the USA used classification and regression tree modelling of 250 m spatial resolution MODIS imagery and forest inventory data to estimate *AGB*, its uncertainty, and forest probability maps (Blackard et al., 2008). The study also used the National Elevation Dataset (NED, Gesch et al., 2002) and land cover map layers from the National Land Cover Dataset (NLCD92, Vogelmann et al., 2001). However, the uncertainty in *AGB* was only based on the relative error of the modelled prediction, lacking an error propagation approach which would have allowed the incorporation of other sources of uncertainty at pixel scale.

Forest aboveground biomass carbon (*AGBC*) stocks in Mexico for the FAO Forest Resource Assessments were estimated by the Comision Nacional Forestal (CONAFOR). Saatchi, Harris, et al. (2011b) mapped *AGBC* over the whole tropical region for the first time (including Mexico) using satellite datasets at 1 km spatial resolution, and estimated the uncertainty of *AGBC* on a pixel scale by combining the probabilistic outputs generated from the MaxEnt algorithm with data from ICESat GLAS LiDAR footprints and MODIS, quick scatterometer (QSCAT) and SRTM. Later work by Baccini et al. (2012) mapped *AGBC* in the tropics (partially covering Mexico) at 500 m resolution using ICESAT-GLAS LiDAR, MODIS and SRTM, but without spatial uncertainty estimation. These tropical carbon maps for the year 2000 by Saatchi, Harris, et al. (2011b) (hereafter TCM-1) and for the year 2005 by Baccini et al. (2012) (hereafter TCM-2) are consistent in their methods but show large discrepancies in *AGB* (Mitchard et al., 2013). They also disagree with the official carbon estimations for Mexico from *in-situ* data (FAO, 2010a) and with ground data and locally calibrated products in other regions (Hill, Williams, Bloom, Mitchard, & Ryan, 2013, Mitchard et al., 2014; Carreiras, Melo, & Vasconcelos, 2013). These maps have been globally calibrated (continentally in the case of TCM-1) using *AGB* reference data estimated from GLAS height metrics and global or continental allometric models solely based on canopy height, which might explain why they do not fully capture the spatial variation of *AGB*. The most recent assessment covering the whole of Mexico is the map of forest aboveground carbon stocks for the year 2005 by Cartus et al. (2014) (hereafter MRF) at 30 m resolution from a Random Forest (Breiman, 2001) algorithm. The studies described above follow different approaches, which have resulted in substantial differences in the total amount of carbon stocks in Mexico (Table 1). TCM-1 estimates a carbon stock in Mexico 0.71 Gt C higher than MRF. This difference can be converted to 2.6 Gt CO_2-e (carbon dioxide equivalent) and translated to an economic value of $23.9 billion using the average price of $9.2/t CO_2-e (Peters-Stanley, Hamilton, & Yin, 2012).

In this study, a MaxEnt approach is used to estimate *AGB* at country-level with locally calibrated field inventory data and compared to existing *AGB* products. The contribution of different input datasets (ALOS PALSAR, MODIS, and SRTM) is analysed. The resulting *AGB* map is used to estimate forest carbon stocks in Mexico and their uncertainty. The probability of a pixel belonging to the forest class is estimated, and a systematic error propagation approach to assess the uncertainty of *AGB* estimates at pixel scale is described. The forest probability layer ranges from 0% (uncertain) to 100% (certain). The forest probability layer allows the assessment of the uncertainty associated with the metric estimates of *AGB*, and the uncertainty in the binary forest/non-forest mask. The results from using different forest masks based on a similar forest definition (i.e. FAO) but originating from different sensors are also presented. Sources of uncertainty in the approach are discussed and compared to previous studies.

2. Study area and data

2.1. Study area and AGB reference data

Mexico's topography, climate, and history of human land use are extremely diverse, leading to a wide variety of different forest habitats (Fig. 1). The north of the country is covered by a mosaic of dry evergreen forest, deciduous forest and shrub vegetation, while the central region and the south are covered by a diverse mix of evergreen and deciduous forest, cloud forest at high elevations, shrub vegetation, savannahs, mangroves, and evergreen, deciduous and semi-deciduous tropical forests. The Yucatan peninsula is dominated in the north-west by sub-humid or dry deciduous tropical forest, while the south-east is dominated by humid evergreen tropical forest, with mangroves and areas of other hygrophilous vegetation. An increasing gradient of *AGB* is expected to be observed from NW (dry) to SE (humid) of the Yucatan peninsula. Mexico is also one of the countries with the highest biodiversity in the world (Mittermeier, 1997). This biodiversity is mostly concentrated in the tropical forest areas of the country.

Mexico is covered by approximately 65 million ha of forest and 20 million ha of other wooded land (43% of the national territory) (FAO, 2005). The Mexican National Forest and Soil Inventory (INFyS) of CONAFOR is a national inventory database that provides information on the size, spatial distribution and condition of forest resources (SEMARNAT, 2004). This information is used to support the development of national policies for sustainable development and to promote forestry activities. The field plot data from this inventory can be integrated with Earth observation data to map *AGB* over the whole country. Each field plot from INFyS (CONAFOR, 2012b) has a data record spanning 8 years from 2004 to 2012. We use 17,171 plots comprising four 400 m^2 (0.04 ha) sub-plots representing an area of about 1 ha, which are systematically distributed across all forested areas of Mexico. All live trees above 7.5 cm of diameter at breast height were measured within these sub-plots. The sampling distance between centres of the plots is 5 × 5 km in forest and mangroves, and 10 × 10 km in dry tropical forest and semi-arid vegetation. Therefore, a total area of 0.16 ha is sampled at each location and assigned to the overlapping remote sensing pixels of 6.25 ha (250 × 250 m) used in this study. The difference between plot size and pixel size is one source of uncertainty in mapping the forest biomass.

A total of 339 allometric equations and 214 species-specific wood densities were used by CONAFOR (CONAFOR, 2012b; CONAFOR, 2012a) to estimate tree-level *AGB* following a protocol for allometric model selection which prioritises the use of species-specific models and wood densities within their diameter range. If more than one equation is available for

Table 1
Comparison of different carbon stock assessments for Mexico.

Study	Period	Method	Datasets	Total carbon (Gt C)	Mean carbon (t C ha^{-1})	RMSE pixel level (t C ha^{-1})
FAO[a]	2000	Forest inventory	INFyS, LUV	1.75	26.24	N/A
	2005			1.72	26.22	
	2010			1.68	25.93	
TCM-1[b]	2000	MaxEnt	GLAS. MODIS, QSCAT, SRTM	2.24	32.94	±27.3%[*]
MRF[c]	2005	Random Forest	INFyS, LUV, Landsat PTC, ALOS PALSAR, SRTM	1.53	23.61	±14.4
TCM-2[d]	2005	Random Forest	GLAS, MODIS, SRTM	1.95[**]	46.35	±25.0

[a] FAO (2010a)
[b] Saatchi, Harris, et al. (2011b) (TCM-1). 1 km (100 ha) pixel size. VCF 10% cover as forest mask.
[c] Cartus et al. (2014) (MRF). 30 m (0.09 ha) pixel size. LUV as forest mask
[d] Baccini et al. (2012) (TCM-2). 500 m (25 ha) pixel size.
[*] Relative error.
[**] Country half covered.

each tree the equation with highest R^2 or with the closest regional relevance is selected. If no species-specific model is available, the same procedure is followed at higher levels (genus and forest type). Due to the lack of species- or genus-specific allometries for all tree species, generalized models are used (Chave et al., 2005; Brown, 1997) for approximately half of the plots in the INFyS database (Cartus et al., 2014).

Most plots have been measured twice during this 8 year period. In these cases the average of both measurements was used if the second measurement was higher or relatively similar to the first measurement. This was done to better represent the *AGB* in the reference year of 2008 of the INFyS measurements (2004–2012). If the second measurement was significantly lower, it was assumed that the forest was cleared during the period, and therefore the plot was removed from the analysis. Several primary units were also excluded due to the lack of geographical coordinates. A total of 16,613 plots from the INFyS dataset were retained for the final analysis. The primary sampling sites from INFyS were divided into a training dataset (15,348 plots) and a validation dataset (1265 plots), comprising 90% and 10% of the data respectively (Fig. 1).

2.2. Remote sensing data

Remote sensing imagery (Table 2) was collected, mosaicked, co-registered and aggregated to 250 m spatial resolution. Scatterplots and spatial trend plots were used to assess the correlation of *AGB* to the remote sensing data layers. MODIS vegetation index (VI) 16-day products (MOD13Q1) (NASA, 2008) over Mexico (9 mosaic tiles) were acquired from the USGS (USGS, 2012). MODIS VI layers were used to generate NDVI, EVI, Blue, Red, MIR, and NIR layers for the greenest vegetation period. The highest NDVI (greenest) values in Mexico occur between July and August; here the period from June to September is used. Maximum values of NDVI and EVI products as well as averages of the reflectance bands were then generated for this period using the reliability layers to discard pixels covered by snow, ice or clouds. MODIS vegetation continuous fields—VCF (MOD44B) collection 5 data (DiMiceli et al., 2011) were acquired from the Global Land Cover Facility (GLCF) to generate a mosaic over Mexico.

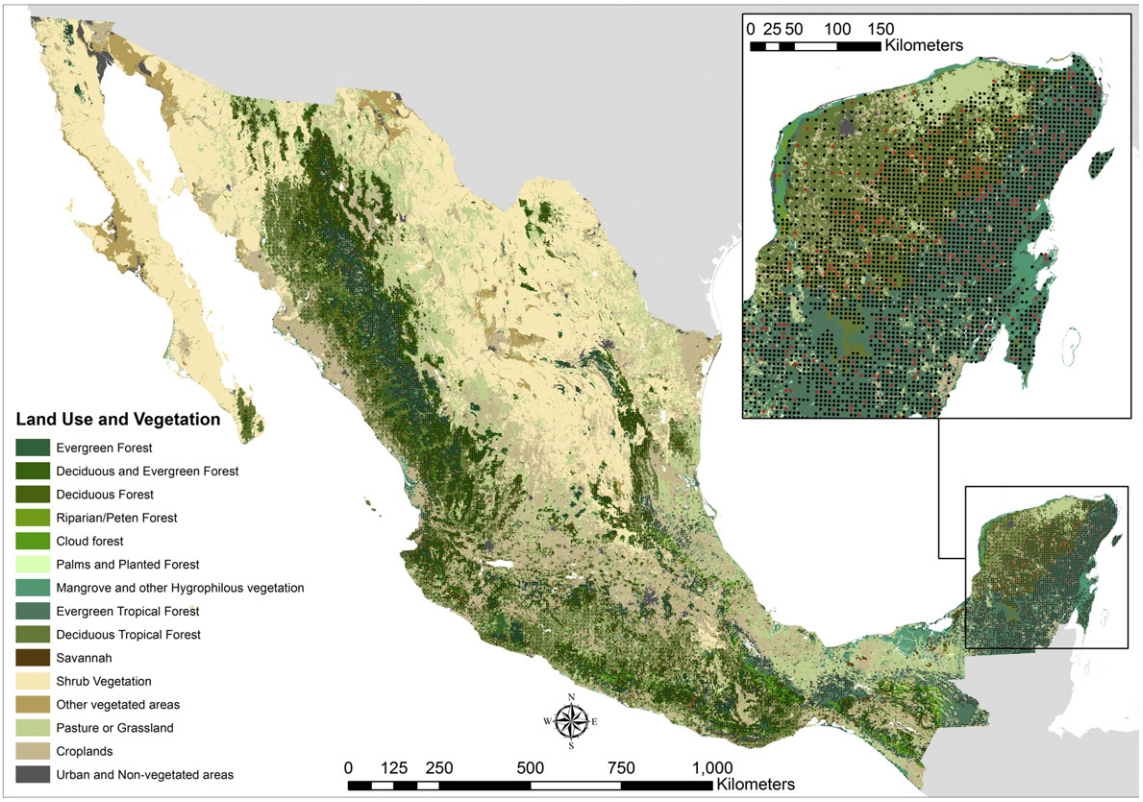

Fig. 1. Land use and vegetation map of Mexico (INEGI, 2009). Training dataset (black dots) and validation dataset (red dots) comprising 90% and 10% of the INFyS data respectively.

Slope-corrected, orthorectified, and radiometrically calibrated ALOS PALSAR backscatter intensity mosaics at 50 m resolution for both polarisations (HH and HV) were obtained from JAXA (JAXA, 2014) for the years 2007, 2008, and 2009. A destriping process (Shimada & Isoguchi, 2002) is applied by JAXA to equalize the intensity differences between neighbouring strips due to seasonal and daily differences in surface moisture conditions. Strips with remaining significant striping were excluded. Multi-temporal averaged mosaics were aggregated to 250 m resolution to reduce speckle. The K&C-FNF product at 100 m resolution was also obtained from the same repository and aggregated at 250 m resolution based on a majority rule. The Mexican Land Use and Vegetation map (LUV) vector file developed by INEGI (INEGI, 2014b) was also acquired. A gap-filled version of the Shuttle Radar Topography Mission—SRTM (USGS, 2006) at 250 m resolution was obtained from the International Centre for Tropical Agriculture (CIAT) (Jarvis, Reuter, Nelson, & Guevara, 2008). The SRTM elevation was used to estimate slope and aspect of the terrain which were included as predictors.

2.3. Validation data

The INFyS dataset was stratified in a random sampling framework in seven forest types (evergreen, deciduous, mix evergreen–deciduous, cloud forest, mangrove, evergreen tropical forest and deciduous tropical forest) and further within three *AGB* ranges (quantiles for low, medium and high *AGB*). 10% of the plots from each stratum were set aside. This dataset (1265 plots) was excluded from the training of the MaxEnt algorithm and was used instead to validate the *AGB* map. Additionally, an independent forest/non-forest binary validation dataset distributed systematically in a triangular mesh pattern over Mexico was generated. These 198 validation points were 100 km apart. Each point was assigned to the class "forest" or "non-forest" based on a visual classification of a square area with 300 m of side around the point using Google Earth high resolution multi-temporal imagery from 2008 and the closest available years. In this task the LUV dataset was also used as a reference of the potential vegetation for each site. Tree canopy cover (using FAO's canopy cover definition) of more than 10% of the area was defined as "forest". The different forest masks were validated against this dataset.

3. Methods

3.1. Modelling approach

There are different parametric and non-parametric approaches to extrapolate field plot-derived estimates of *AGB* to global and regional scales using remote sensing imagery. The MaxEnt algorithm used here allows the combination of different sensor types to scale up the field plot measurements (Phillips, Anderson, & Schapire, 2006, Phillips, Dud, & SCHAPIRE, 2004). MaxEnt is a non-parametric algorithm that generates spatial predictions of probability distributions based on an incomplete set of information (Phillips et al., 2006; Phillips et al., 2004; Li & Guo, 2010). It was originally developed for statistical modelling of species presence data without full knowledge of species absences, and identifies relationships between explanatory environmental variables (here the remote sensing data layers) and the response variable (here *AGB*).

Several studies (Elith et al., 2011; Hastie, Tibshirani, Friedman, & Franklin, 2005, Wollan, Bakkestuen, Kauserud, Gulden, & Halvorsen, 2008) have found that MaxEnt is reliable and performs well in comparison to other machine learning algorithms and is more stable using correlated variables than for example stepwise regression. Removing correlated variables or pre-processing of covariates is therefore less important for MaxEnt. Saatchi, Harris, et al. (2011b) presented a multi-sensor approach that uses MaxEnt to map the spatial distribution of *AGB* at 1 km spatial resolution for the entire tropical biome. An advantage of this approach is the explicit treatment of the uncertainty of the *AGB* estimation on a pixel scale, allowing the incorporation of different sources of error and the analysis of the contributions of each remote sensing data layer across the *AGB* estimation range.

MaxEnt estimates the probability distribution of discrete classes with maximum entropy (closest to a uniform distribution) subject to the constraints established by the input information (remote sensing data layers) (Phillips et al., 2006). In 1000 iterations for each *AGB* class the weights for combining the remote sensing data layers are adjusted to maximise the average sample likelihood (training gain), and to estimate the distribution over the whole region. This approach is an adaptation of the method by Saatchi, Harris, et al. (2011b), which uses the probabilities calculated by the MaxEnt algorithm to estimate *AGB* and its uncertainty (Fig. 2). Here, we use *AGB* field plots and allometric models to calibrate the algorithm regionally instead of Saatchi's approach to estimate *AGB* from GLAS LiDAR footprints (using a 2-step modelling from LiDAR metrics to canopy height, and then to *AGB*) for a large continental calibration. In addition, a forest probability layer was generated from this method, instead of using MODIS VCF for masking forest cover.

The implementation of this probabilistic method required the set of *AGB* training plots to be classified into discrete *AGB* classes. The minimum number of plots per class was 100. Thus, the training dataset was divided into eleven classes in 20 t ha^{-1} intervals (1–20 t ha^{-1}, 21–40 t ha^{-1},..., >200 t ha^{-1}). These *AGB* classes were used in combination with the remote sensing data layers in MaxEnt to create eleven *AGB* class probability layers. *AGB* of each pixel was calculated as the weighted average *AGB* per pixel with the probabilities as weights (Eq. 1). The uncertainty of the *AGB* prediction ($\varepsilon_{prediction}$) was calculated from the root mean square error ($\sigma_{\widehat{AGB}}$) per pixel (Eqs. 2 & 3). The following equations were used (Saatchi, Harris, et al., 2011b):

$$\widehat{AGB} = \frac{\sum_{i=1}^{N} P_i^n AGB_i}{\sum_{i=1}^{N} P_i^n} \tag{1}$$

$$\varepsilon_{prediction} = \sigma_{\widehat{AGB}} / \widehat{AGB} \times 100 \tag{2}$$

$$\sigma_{\widehat{AGB}} = \sqrt{\frac{\sum_{i=1}^{N} \left(AGB_i - \widehat{AGB}\right)^2 P_i}{\sum_{i=1}^{N} P_i}} \tag{3}$$

where $\widehat{AGB}$ is the *AGB* prediction per pixel, and P_i is the probability estimated by MaxEnt for each *AGB* range AGB_i (average value within class i). The power *n* of the probability is used to weight the predicted value

Table 2
List of remote sensing products and layers used in this study.

Remote sensing product	Resolution	Sensor	Layers
16-Day MODIS VI (2008)	250 m	MODIS	NDVI, EVI, blue, red, MIR, NIR
ALOS PALSAR mosaic (2007–2009)	50 m	ALOS PALSAR	HV, HH
Digital elevation (2000)	90 m	SRTM	Elevation, slope, aspect
Vegetation continuous fields (2008)	250 m	MODIS	Percent tree cover
K&C-FNF (2008)	100 m	ALOS PALSAR	Forest / non-forest

VI, vegetation indices; NDVI, normalized difference vegetation index; EVI, enhanced vegetation index; SRTM, Shuttle Radar Topography Mission; MIR, mid-infrared; NIR, near-infrared; FNF, forest/non-forest.

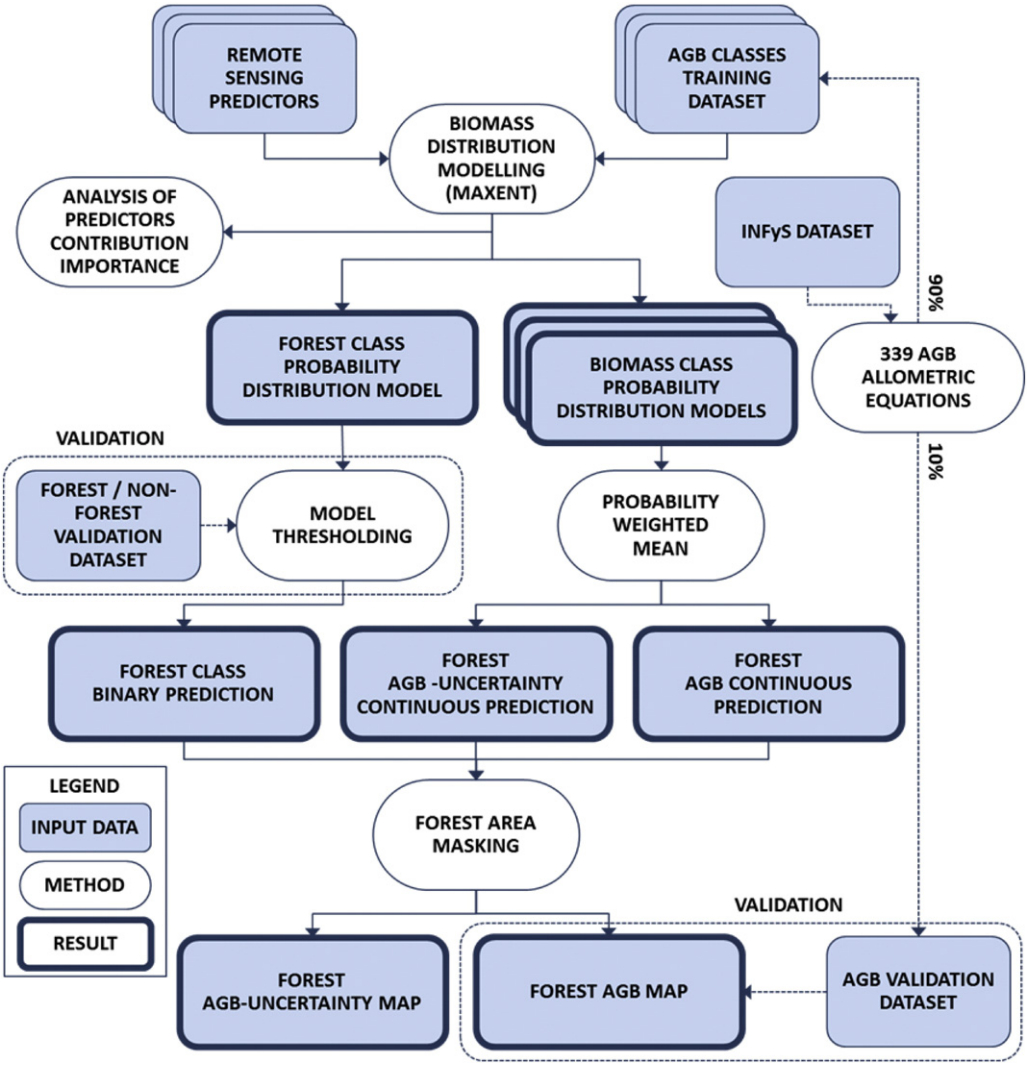

Fig. 2. Schematic of the MaxEnt *AGB* distribution model approach used in this study. Remote sensing predictors include optical, SAR and DEM datasets.

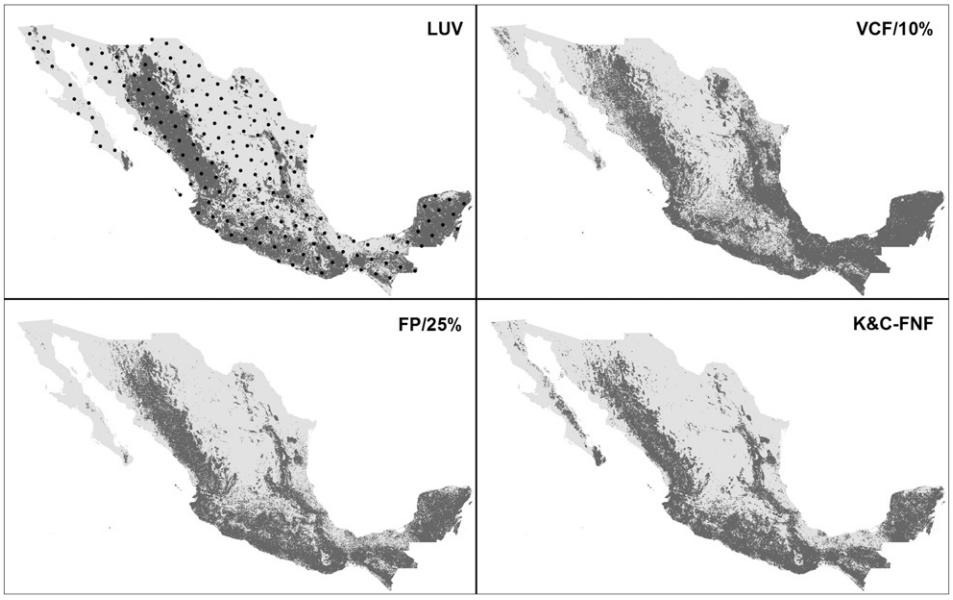

Fig. 3. Forest extent defined by the LUV map, by the $FP_{25\%}$, by MODIS VCF with 10% tree cover threshold (hereafter $VCF_{10\%}$), and by K&C-FNF. Dark grey represents forest and light grey non-forest. The location of validation points ($n = 198$) is displayed in the LUV map.

Table 3
Summary statistics of final maps using different forest masks.

Forest mask (threshold)	Forest probability (%)	Forest area κ	Forest cover (M ha)	Average *AGBC* (t C ha^{-1})	Average uncertainty (±%)	Total *AGBC* (Gt C)
$FP_{25\%}$	0.47	0.83	77.25	21.8	49.3	1.69
$FNF_{-14.5\ dB}$	0.45	0.78	80.21	20.6	49.9	1.65
K&C-FNF	0.44	0.72	73.80	21.2	51.1	1.56
$VCF_{10\%}$	0.36	0.66	97.80	19.6	57.7	1.92
LUV	0.43	0.56	67.27	21.8	50.2	1.47

towards the maximum probability closest to the true value when other probabilities are small. This study used $n = 3$. As explained in Saatchi, Harris, et al. (2011), $n = 3$ preserves the skewness in the distributions for each pixel, and produce the best results based on cross-validation tests.

The total uncertainty at pixel level is composed of four sources of error which are assumed to be random and independent. These are propagated using the following equation:

$$\varepsilon_{AGB} = \left(\varepsilon^2_{measurement} + \varepsilon^2_{allometry} + \varepsilon^2_{sampling} + \varepsilon^2_{prediction}\right)^{1/2}, \quad (4)$$

The measurement error of tree level parameters such as diameter and tree height ($\varepsilon_{measurement}$) averaged at plot scale (Chave et al., 2004) was assumed to be 10% (Mitchard et al., 2011). The error in estimating *AGB* using allometric equations ($\varepsilon_{allometry}$) with species-specific wood densities and diameter ranges is on average 11% based on Chave et al. (2004). The error originating from the variability of *AGB* within the 6.25 ha pixel area ($\varepsilon_{sampling}$) depends on the size of the plots used to upscale the *AGB* measurements to the pixel scale. This error is approximated using data from Chave et al. (2003) on the *AGB* variability of a 50 ha plot. Chave et al. (2003) use a sample size equation for the 95% confidence interval and found that at least 160 plots of 0.04 ha area are needed to estimate *AGB* of a 50 ha plot with a ±10% uncertainty. This means that a sampling intensity of 12.8% (0.04 × 160/50) is needed. By assuming the same variations in the 6.25 ha pixel, the number of 0.04 ha plots needed to reach the same sampling intensity will be 20. Each pixel uses one INFyS primary unit containing four 0.04 ha sub-plots (0.16 ha). Thus, the uncertainty of the *AGB* estimation will increase to 22.4% ($10 \times \sqrt{20/4}$). This value is also similar to the error estimated for 0.2 ha plots in old-growth forest in La Selva Biological Station in Costa Rica (Saatchi, Marlier, Chazdon, Clark, & Russell, 2011a). The error calculated for each pixel from the prediction probabilities of MaxEnt ($\varepsilon_{prediction}$) also accounts for the representativeness of the sampling sites of the true distribution of *AGB* in the region (Saatchi, Harris, et al., 2011b).

In order to avoid non-zero biomass estimates in non-forest pixels, the forest area has to be masked out. The FAO forest definition of forest, ignoring temporally unstocked areas, is used here. As the probability calculated by the MaxEnt algorithm is equal to the Gibbs probability and is proportional to the conditional probability of the class (i.e. forest class) (Li & Guo, 2010), the locations of forest inventory plots can be used as training data to generate a forest probability map (FP). These plots were located in forest areas according to the CONAFOR forest definition. However, only plots with canopy cover above 10% and canopy height above 5 m were used as training data, in accordance with the FAO forest definition (FAO, 2010b) and other forest cover products

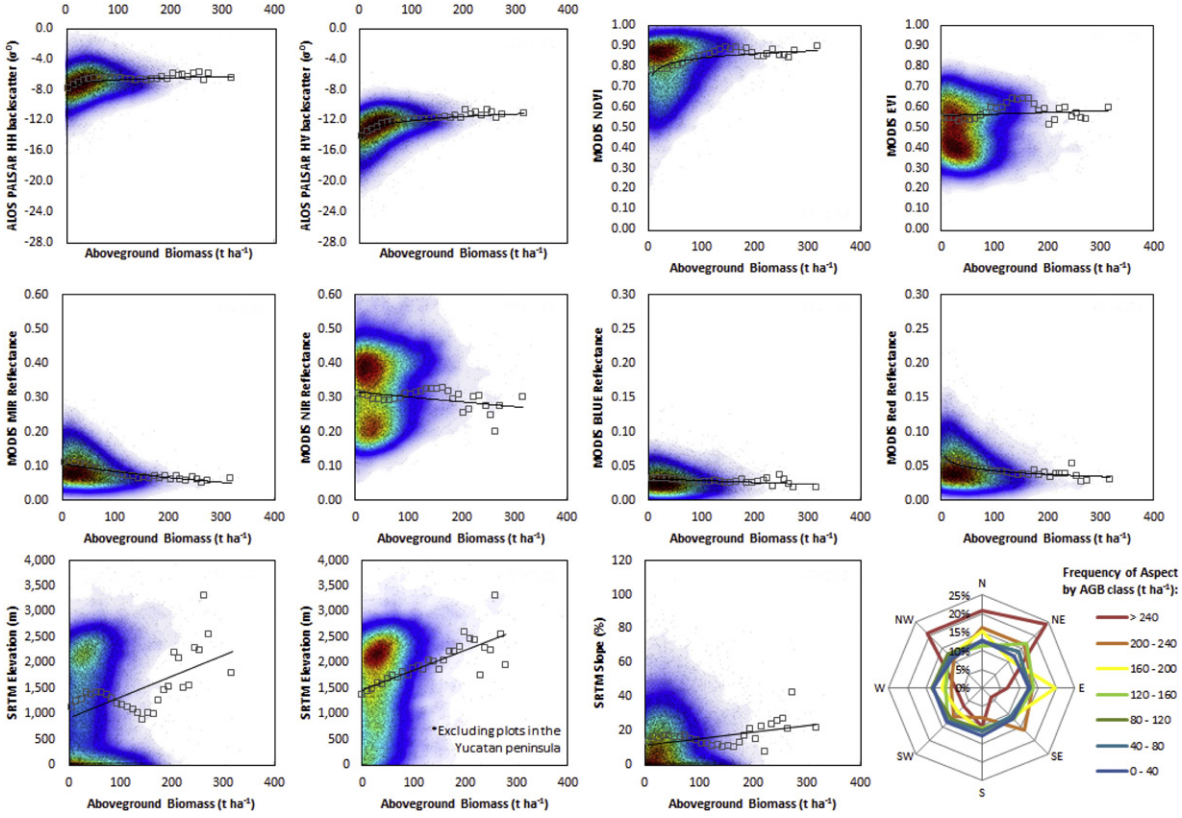

Fig. 4. Scatterplots of INFyS *in-situ* measured *AGB versus* remote sensing variables used in this study. Trend lines are generated from the square points (average value of the variables per each 10 t ha^{-1} interval *AGB* range). Warmer colours indicate higher point density. Frequency spider-diagram per *AGB* class is used for elevation aspect.

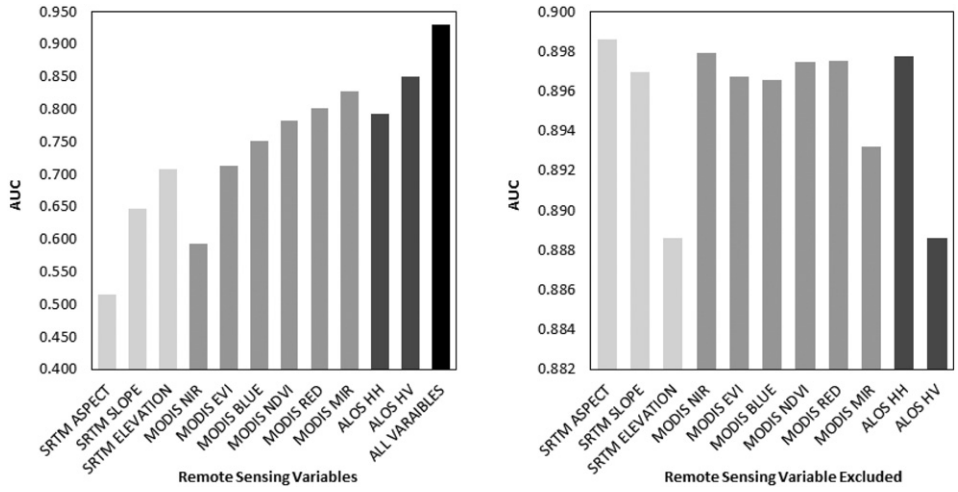

Fig. 5. Average AUC of *AGB* map for single variable models and all variables together (left). Average AUC of *AGB* map for models excluding a single variable (right) (note: y-axis has different scaling).

(MODIS VCF and K&C-FNF). This new plot dataset was then used to train the MaxEnt algorithm. The same remote sensing data layers used to develop the *AGB* and uncertainty maps were also used for this forest class probability map. The resulting map provides a conditional probability of each pixel being forest.

A binary forest/non-forest layer is defined by setting a probability threshold for the pixel belonging to the forest class. Four threshold optimization criteria have been recommended in previous studies: one threshold which maximises the κ coefficient of agreement with the validation dataset (Pearson, Dawson, Berry, & Harrison, 2002); a second where sensitivity (proportion of positives correctly identified) equals specificity (proportion of negatives correctly identified) of the binary classification (Hattab et al., 2013; Freeman & Moisen, 2008); a third that maximises the sum of sensitivity and specificity (Hattab et al., 2013; Freeman & Moisen, 2008); a fourth threshold corresponding to a 5% error of omission (Li & Guo, 2010, Pearson, Dawson, & Liu, 2004). The probability threshold corresponding to the 5% of the error of omission in the training data obtained from the MaxEnt algorithm was 27%, for the equal sensitivity and specificity 46%, and for the maximum sensitivity plus specificity 35%. The highest κ obtained from the validation for the forest masks generated from the FP map occurred for the probability threshold of 25% (i.e. the first threshold optimization criterion listed above). Therefore, a forest/non-forest layer was generated using the lowest threshold (hereafter $FP_{25\%}$).

Other forest masks are also compared to the $FP_{25\%}$ mask (LUV, MODIS VCF, and K&C-FNF). A visual comparison between the forest cover defined by these products shows differences (Fig. 3). The K&C-FNF product is based on a HV backscatter threshold optimized for large areas. A second forest mask was generated from the ALOS PALSAR backscatter layers by optimizing a threshold for Mexico using the validation dataset. The best results were obtained with a HV backscatter threshold of −14.5 dB (hereafter $FNF_{-14.5dB}$). The accuracy of these forest masks was assessed against the forest/non-forest validation dataset. As the accuracy of the $FP_{25\%}$ is highest (Table 3), this mask was used for the final *AGB* map.

3.2. Analysis of remote sensing variables and algorithm performance

The performance of MaxEnt was assessed by bootstrapping 25% of the training data. Jackknife analyses were performed to select the most suitable input data layers for predicting *AGB* and forest cover. The analyses were performed based on the area under the receiver operator curve (AUC) and model gain following Phillips et al. (2006), for both the training and validation data. The same remote sensing variables were used to predict the FP map and the *AGB* class probability layers. Remote sensing layers from three sensors (MODIS, SRTM, and ALOS PALSAR) were also used. The variable importance was analysed with the relative contribution of each variable (data layer) to the MaxEnt model gain. The analysis was performed for each remote sensing data layer and *AGB* class. Models were evaluated using all variables, excluding one variable each time, and using one variable in isolation each time. A permutation analysis was carried out for each remote sensing data layer by random permutation of the training data and re-evaluating the model. A large drop in AUC means that the MaxEnt model depends strongly on that variable. The drop in AUC was then normalized to relative values.

3.3. Uncertainty analysis and comparisons at municipality and state level

The independent validation dataset (10% INFyS plots) was used. The uncertainty map generated by the MaxEnt error propagation approach

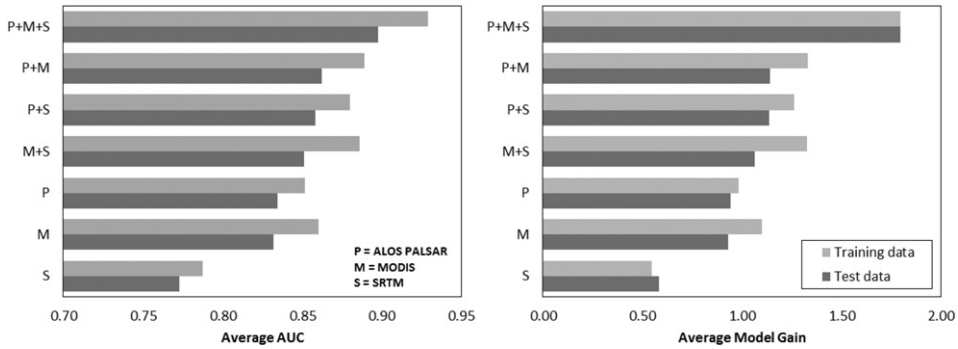

Fig. 6. Average AUC (left) and average model gain (right) of *AGB* map for training and test data..

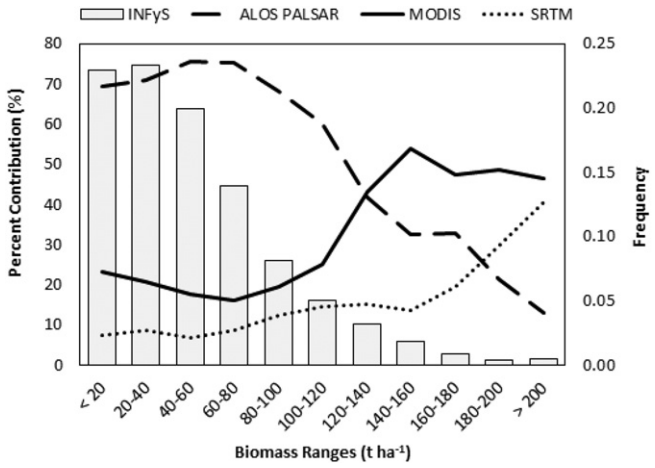

Fig. 7. Percent contributions to the *AGB* map per biomass range (lines) and frequency INFyS plots (columns).

was used to analyse the uncertainty in *AGB* levels and forest types. A multi-scale analysis of total carbon stocks derived by the INFyS dataset and by the *AGB* map derived using the MaxEnt approach was carried out following Cartus et al. (2014) at municipality and state levels. The average *AGB* per ha for each municipality/state was calculated as the mean of the values from the INFyS plots, weighted by the forest type area (coniferous forest, mixed coniferous-broadleaved forest, broadleaved, humid tropical forest, dry tropical forest, and mangrove forest). The INEGI land use and vegetation map was used for this purpose.

3.4. Comparison with previous studies

The present study (hereafter AGB-MEX) was compared to previous studies of *AGBC* stocks in Mexico (Saatchi, Harris, et al., 2011b, Baccini et al., 2012; Cartus et al., 2014; FAO, 2010a). *AGBC* is calculated in this study by applying the Mexican average *AGB*-to-carbon ratio of 0.48. AGB-MEX used a forest inventory plot dataset (INFyS) based on a systematic stratified sampling design with a sampled area of 0.16 ha per plot to train 250 m (6.25 ha) pixels (2.5% sampled area within the pixel). TCM-1 used a random sampling design (ICESat footprints) and at least five 0.4 ha GLAS LiDAR footprints (2 ha) to train the 1 km (100 ha) pixels (>2% sampled area). AGB-MEX uses L-band SAR with a wavelength that physically interacts more with forest *AGB* components (replacing the Ku-band used in TCM-1). The AGB-MEX approach also incorporated a FP map to produce a more accurate forest mask than in TCM-1 (which used MODIS $VCF_{10\%}$), and provided spatial information on the accuracy of the mask. The TCM-2 also used *AGBC* estimated from GLAS LiDAR footprints to train a Random Forest algorithm with 500 m resolution MODIS imagery. The *AGBC* estimates from these studies were compared by assessing total *AGBC* stock, mean *AGBC* per ha, histograms and spatial distribution across the entire Mexican territory. Moran's I was also used to assess the spatial pattern (spatial clustering) of the *AGB* predictions of each map over forest areas (delineated by the LUV mask) within each state.

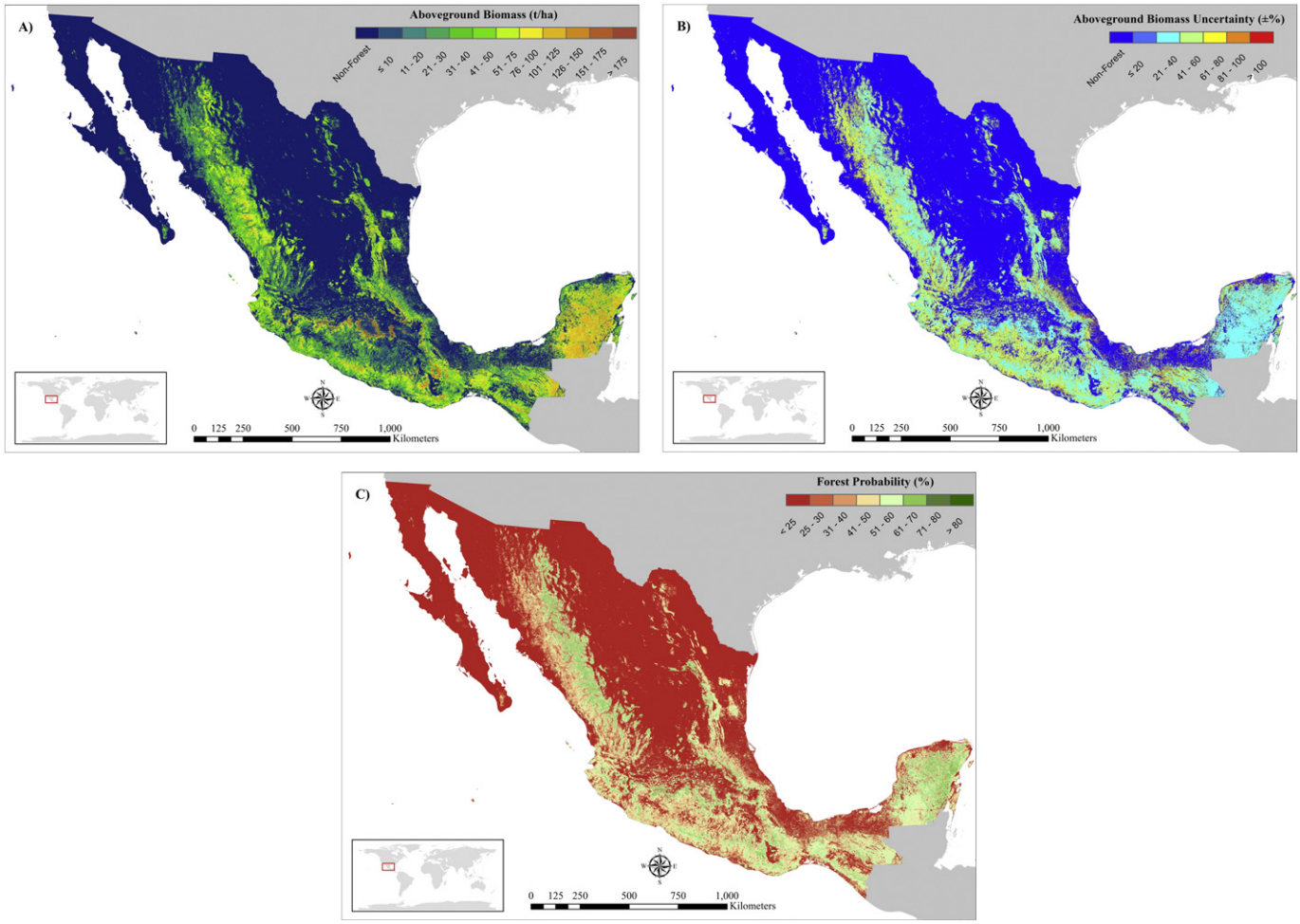

Fig. 8. A) Aboveground biomass, B) biomass uncertainty, and C) forest probability maps for Mexico *ca.* 2008. Maps are masked by a 25% probability threshold.

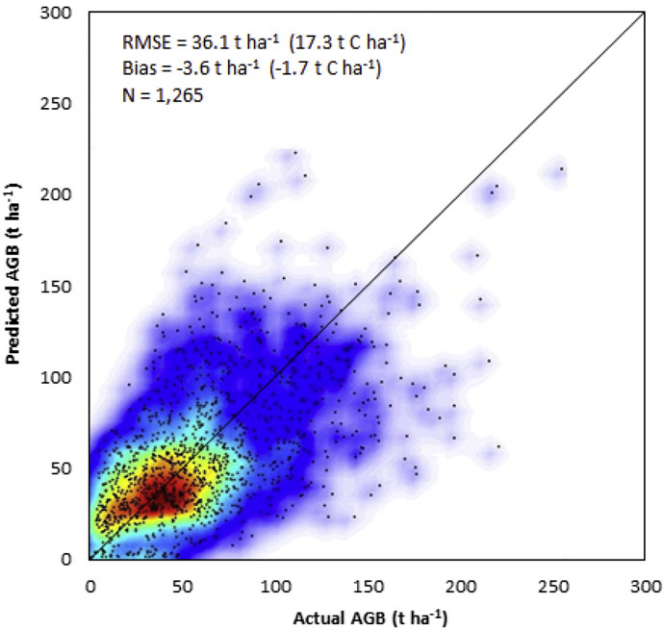

Fig. 9. Validation of the *AGB* map using an independent plot dataset. Warmer colours indicate higher point density. Solid line: y = x.

4. Results and discussion

4.1. Variable importance and model performance

Scatterplots of the INFyS dataset were used to assess the correlation between *AGB* and the remote sensing data layers (Fig. 4). The analysis of *AGB* by elevation band shows two point-cloud clusters. When excluding plots from the Yucatan peninsula only one of the clusters remains, showing a possible altitudinal gradient. The Yucatan peninsula in the south-west of the country contains a wide range of *AGB*, including some of the highest *AGB* measured in Mexico. This area is predominantly covered by humid tropical forest and the terrain is mostly flat and near sea level in altitude. A positive trend is observed in the rest of the country with increasing elevation for the INFyS data. The most strongly correlated remote sensing data layer to biomass is the ALOS PALSAR HV-polarized backscatter followed by the MODIS MIR reflectance (Fig. 4).

Jackknife analyses based on AUC changes were used to assess the remote sensing data layers. MaxEnt models were run with each single variable in isolation. Then, models using all variables together were run excluding one single variable each time. The former shows the importance of each variable on its own to predict *AGB*, while the latter shows which variables contain more unique information that was not included in the other variables. The results show that ALOS PALSAR HV and MODIS MIR were the most important data layers used on their own, while SRTM ASPECT and MODIS NIR were the least important. The ALOS PALSAR HV and SRTM ELEVATION layers contain more unique information, because the AUC drops the most when these variables are excluded. In contrast, excluding SRTM ASPECT or MODIS NIR results in the smallest decreases in AUC (Fig. 5).

To assess the relative importance of each remote sensor, AUC and model gain analyses were performed, grouping input layers by remote sensing instrument: ALOS PALSAR, MODIS, and SRTM (Fig. 6). Each column represents the average AUC and model gain obtained from the probability class layers by running the MaxEnt algorithm with different sets of input layers. The combination of the three sensors showed superior prediction power over the use of single sensor or two sensors (Fig. 4), so this combination was used to develop the *AGB* and FP maps for Mexico. The algorithm performance of the final *AGB* class probability layers using the combination of ALOS PALSAR, MODIS, and SRTM products showed an average AUC = 0.93 (training data) and AUC = 0.90 (validation data), and for all cases $P < 0.001$. The AUC for the FP map was 0.82 (training data) and 0.81 (validation data), with $P < 0.001$.

The variable importance analysis of the remote sensing data layers shows that the main input layers contributing to the MaxEnt prediction of *AGB*, when combined together, were ALOS PALSAR HV, MODIS MIR and SRTM ELEVATION. This is expected, as those were the data layers with a high information content that was not provided by any other layer. MODIS MIR has a higher explanatory power for *AGB* than

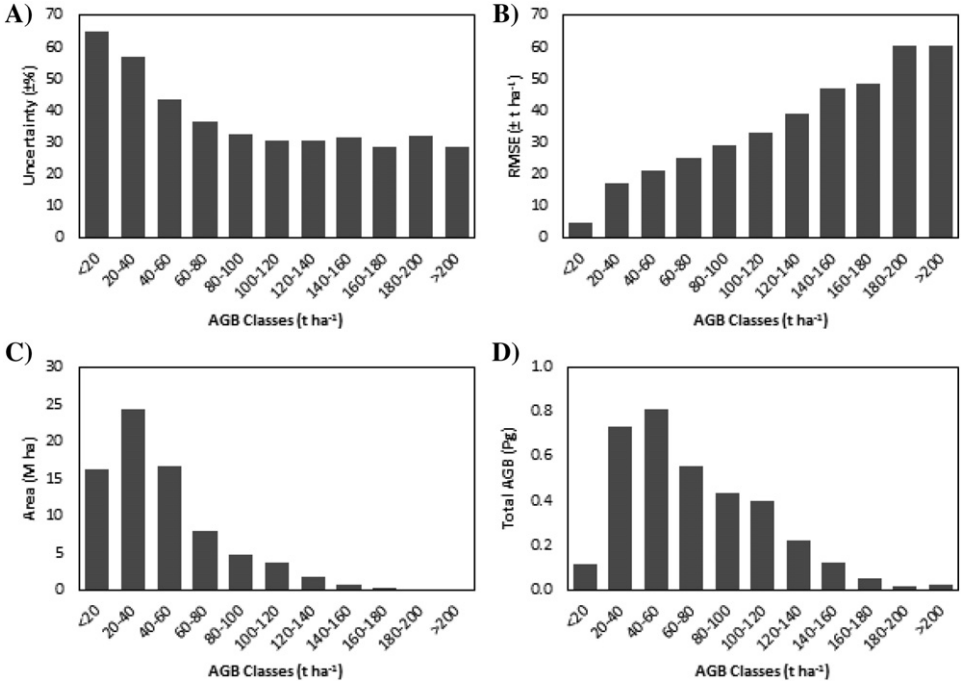

Fig. 10. A) Uncertainty, B) RMSE, C) total Area, and D) total *AGB* by *AGB* class for the AGB-MEX map.

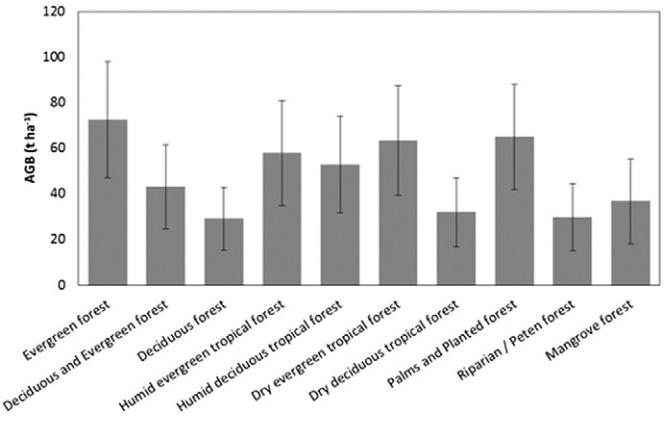

Fig. 11. Average *AGB* and its associated uncertainty per pixel by forest type in Mexico.

vegetation indices such as NDVI. This agrees with recent studies that suggested a correlation of optical image bands (Landsat, MODIS) with *AGB* beyond the theoretical saturation level due to canopy closure, especially in the infrared bands (Baccini et al., 2012, Avitabile et al., 2012), which are sensitive to shadow and moisture. Due to the high correlation between data layers from the same sensor, the remaining layers have lower importance. To address this problem, the analysis is also performed with grouping the variables by sensor.

Overall percent contributions per sensor and permutation importance values showed very similar results. The overall percent contributions of ALOS PALSAR, MODIS VI and SRTM were 50.9%, 32.9%, and 16.2% respectively, while permutation importance values were 49.9%, 37.7%, and 12.4%. In the case of the FP map, the percent contribution of ALOS PALSAR is 77.5%, while MODIS VI and SRTM contributions are 16.8% and 5.6%. Permutation importance values for the FP map were 56.7%, 32.3% and 11.0%. These results contrast with a previous study in Mexico that used optical Landsat percent tree cover, SAR ALOS PALSAR, and SRTM to map carbon stocks, and found that the optical layer was the most important predictor (Cartus et al., 2014).

When exploring the contribution of each remote sensing instrument to the *AGB* class probability layers, it becomes clear that ALOS PALSAR was the most important data layer for *AGB* classes up to 100–120 t ha^{-1} and was still very relevant up to 180 t ha^{-1} (Fig. 7). Above 120 t ha^{-1} MODIS becomes more important and is eventually replaced by SRTM above 180 t ha^{-1}.

The decline in the contribution of ALOS PALSAR to the estimation of *AGB* above 100–120 t ha^{-1} can be explained by the saturation of L-band backscatter at high biomass (Wagner et al., 2003; Mitchard et al., 2009). After the saturation threshold the weight of the estimation fluctuates between data layers. None of the data layers on its own can predict the amount of *AGB* after this point. MODIS optical imagery, as previously mentioned, might contain information in the MIR band which allows an estimation of higher *AGB*. The large contribution of SRTM to the highest *AGB* ranges (above 160 t ha^{-1}) is notable, which is due to the specific distribution of forest *AGB* in Mexico across the topographic gradient, and which has also been observed in a previous study (Cartus et al., 2014). Some of the highest values of *AGB* per ha in Mexico occur at the highest altitudes and slopes (and precipitation), where Ayarín and Oyamel forests are located (from 1500 m to 2000 m altitude). These forests are characterised by tree species such as *Pseudotsuga*, *Picea* and *Abies* and canopy heights above 30–40 m. The lowest *AGB* usually occurs in the lower-lying areas with relatively flat terrain. The only exception to this gradient is the Yucatan peninsula, where high *AGB* values can be found at low elevation with flat terrain.

4.2. Final AGB & uncertainty maps

Different forest masks were used to create *AGB* maps of Mexico. The total *AGBC* estimated for Mexico using the LUV was 1.47 Gt C, which increases by 30% to 1.92 Gt C when using the $VCF_{10\%}$ forest mask (Table 3). It is apparent that $VCF_{10\%}$ tends to overestimate forest cover in comparison with the other products due to the misclassification of areas such as croplands, grassland and other sparse vegetated areas such as forest, generating artificially inflated values of forest carbon stocks. This result shows that the use of different forest masks can have a significant effect on the total forest carbon stock estimated for a country. The carbon stock estimated using the LUV mask is lower than the official 1.68 Gt C reported to FAO (FAO, 2010a), but close to Cartus et al. (2014) estimations of 1.53 Gt C. The difference between forest masks is up to about 30 million ha in forest extent and 0.45 Gt C in total carbon stocks, which can be converted to 1.65 Gt CO_2-e and an economic value of $15.2 billion.

The *AGB* map (Fig. 8) using the $FP_{25\%}$ forest mask presents the highest κ and forest probability, and the lowest average uncertainty at pixel scale (Table 3). The AGB-MEX map estimates the total forest cover as 77.25 M ha, from which a total *AGBC* stock for Mexico of 1.69 Gt C can be inferred, by summing up the total *AGB* of all forest pixels and using the *AGB*-to-carbon ratio (0.48). The uncertainty at national level can be calculated by increasing the sample area and propagating the pixel errors from pixel to national scale. The relative uncertainty is constrained below ±1% for the entire AGB-MEX map for Mexico.

The AGB-MEX map was validated against the independent plot dataset (10% INFyS dataset) resulting in a R^2 of 0.31 for the whole

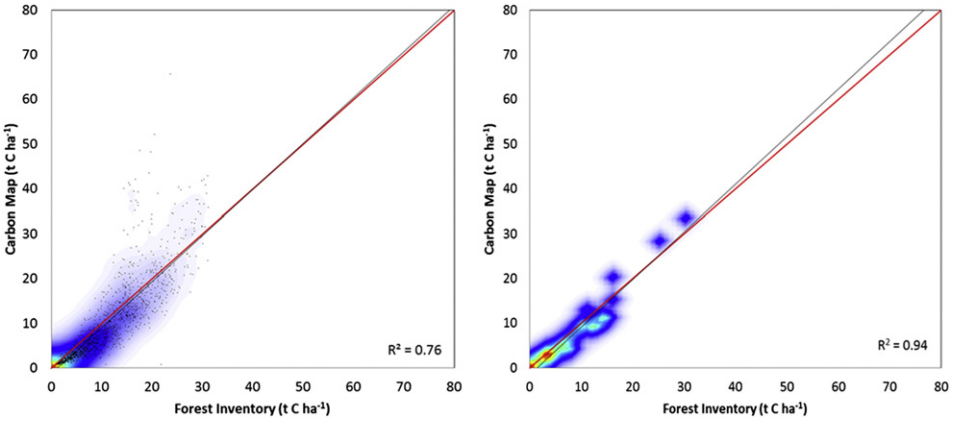

Fig. 12. Comparison of the average carbon estimated from the AGB-MEX map and the INFyS data at municipality (left) and state level (right) following the same approach as in Cartus et al. (2014). Warmer colours indicate higher point density. Red line: y = x.

country. The RMSE and bias at pixel scale were 36.1 t ha^{-1} (17.3 t C ha^{-1}) and −3.6 t ha^{-1} (−1.7 t C ha^{-1}) (Fig. 9).

The highest uncertainty values primarily occur in the lowest *AGB* ranges (Fig. 10) where the sub-pixel variability (i.e. vegetation gaps or other non-forest cover within the pixel) plays an important role. This error originates from the difference of size between the plots used as *AGB* reference data and the pixel size of the remote sensing imagery ($\varepsilon_{sampling}$ in this study). The area covered by *AGB* below 20 t ha^{-1} across Mexico has a considerable extent, but the total amount of *AGB* present in those areas is relatively small in comparison (Fig. 10). Nevertheless, these areas contribute to most of the uncertainty showed by the AGB-MEX map. Some of these pixels are areas with small amounts of sparse woody vegetation encroachments which may have a 10% canopy cover, but in many cases cannot be considered a forest in the sense of FAO as those have to be of at least 0.5 ha or 20 m in width which is below the pixel size used in this study. However, there is no clear definition of forest cover based on a threshold of forest biomass estimated by remote sensing. A biophysical definition of forest would be useful to REDD+. The high uncertainty in those areas gives an insight into the challenges of assessing *AGB* changes between different periods for areas with low biomass density. This error is mostly originating from the plots used to train MaxEnt. A 6.25 ha pixel size is much larger than the INFyS plot area (0.16 ha per 1 ha) used to upscale the *AGB* measurements. The error associated with the *AGB* variability at sub-pixel scale ($\varepsilon_{sampling}$) leads to a very high uncertainty through error propagation (Eq. 4). This uncertainty could be reduced using larger sample plots (e.g. 1 ha sampled area plots) to reduce the error originated from the sub-plot variability as suggested by previous studies (Saatchi, Marlier, et al., 2011a, Montesano et al., 2014).

Average *AGB* and its uncertainties also vary within forest types (Fig. 11). These differences arise from the MaxEnt algorithm error

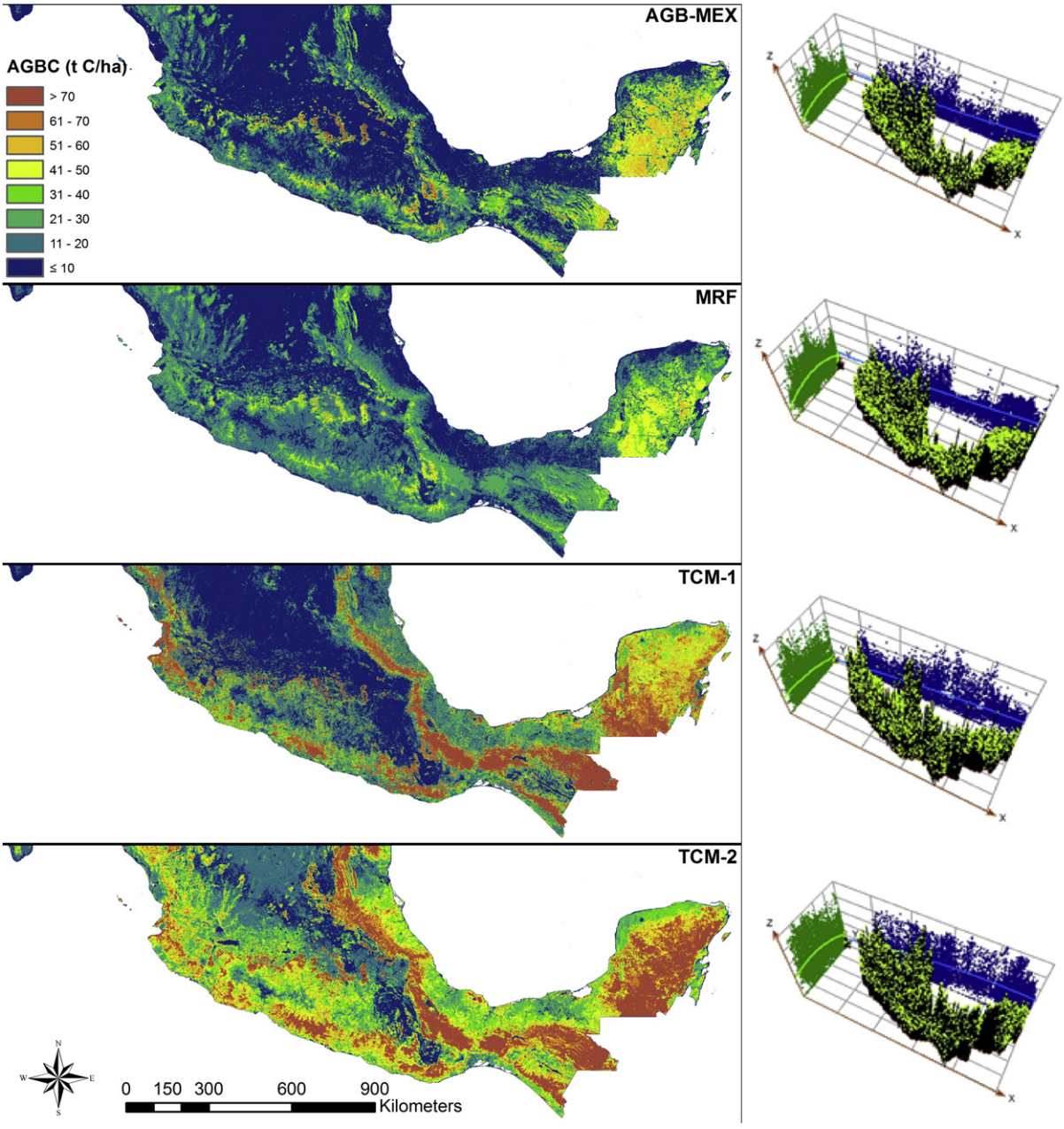

Fig. 13. *AGBC* maps and longitude–latitude *AGBC* trend analysis showing different amounts and spatial distributions of forest *AGBC*. All maps have been aggregated to 1 km spatial resolution for comparison. The location of the INFyS *in-situ* plots were used as sample dataset and represented in the x,y plane, while the *AGBC* values were extracted from each map (AGB-MEX, MRF, TCM-1, and TCM-2) and plotted as the height (z dimension). These values are also projected in the x,z (east–west) and y,z (north–south) planes as scatterplots together with their trend lines (polynomials), allowing to assess the longitudinal and latitudinal trends.

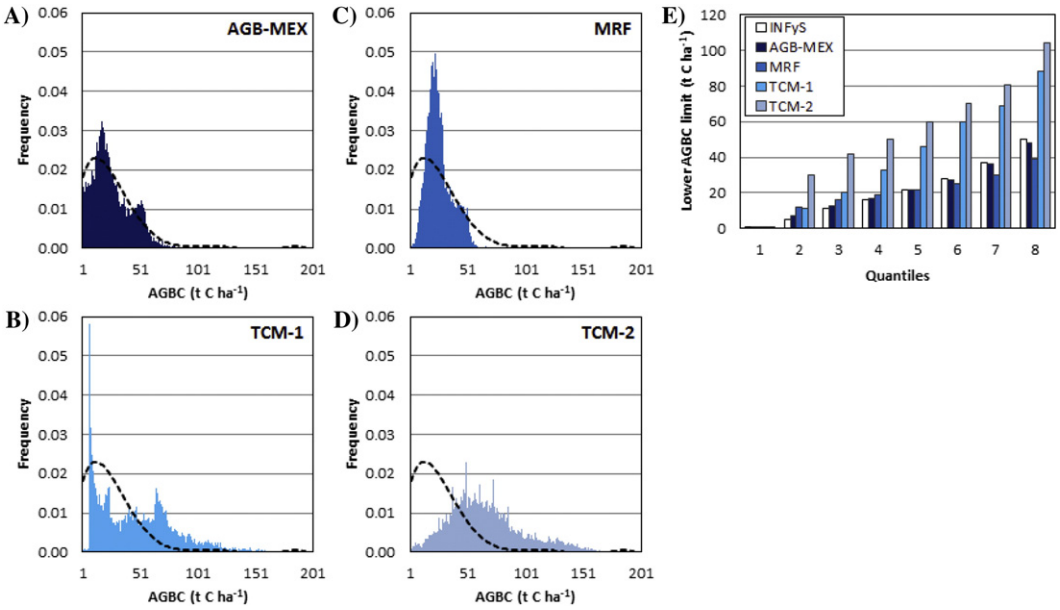

Fig. 14. (A, B, C & D) Histograms of carbon map predictions. Dash line: INFyS *in-situ* plot data histogram. (E) Lower limit of histogram quantiles (same number of occurrences per bin). INFyS location points were used to extract values from the carbon maps and produce their respective histograms.

term ($\varepsilon_{prediction}$) due to weak correlations between remote sensing data layers and *AGB* for certain forest types and *AGB* levels (e.g. caused by signal saturation at high biomass). Evergreen forests have the highest *AGB* per hectare in Mexico. The map shows higher relative errors for deciduous forest than evergreen forest, perhaps due to the seasonality of the broadleaved phenology. Even though the optical data used in this study were acquired within the vegetation growing season, the SAR imagery was acquired in different seasons. The forest structure and hence the backscatter signal from deciduous trees under leaf-on or leaf-off conditions will be different. Evidence for this effect is shown by the correlation between L-band SAR backscatter and leaf area index (Dabrowska-Zielinska et al., 2014; Canisius & Fernandes, 2012, Kovacs et al., 2013). Wetlands also increase the uncertainty, because of the soil moisture effect on radar backscatter. The use of additional SAR wavelengths or texture information generated from the SAR data might better characterise forest structure and can contribute to better estimations in those forest types. The new BIOMASS satellite mission (Le Toan et al., 2011; ESA, 2012) to be launched in 2020 will be less affected by small scattering elements due to the large wavelength of the P-band sensor.

The agreement between the AGB-MEX map and the Mexican forest inventory data was assessed with a multi-scale analysis. The AGB-MEX map was converted to *AGBC* values using a carbon conversion factor of 0.48. The average carbon stock from the AGB-MEX map showed good agreement with the INFyS field plot dataset at municipality scale (average municipality area $= 1.1 \cdot 10^3$ km^2; $R^2 = 0.76$; RMSE $= \pm 4.4$ t C ha^{-1}), 1), and at state scale (average state area $= 61.7\ 10^3$ km^2; $R^2 = 0.94$; RMSE $= \pm 2.1$ t C ha^{-1}) (Fig. 12). AGB state level estimations can be found in Table A1 of the Appendix.

These results confirm that a locally trained MaxEnt approach can provide accurate estimates at spatially coarse scale. However, this is not the case at the scale of the field plot data (1 ha inventory plots), where relative accuracies such as the ones expected from the BIOMASS mission (Le Toan et al., 2011) are not achieved. The AGB-MEX map presented here has quantified different sources of uncertainty (measurements, allometry, sampling, and remote sensing prediction) at pixel scale using an error propagation model. The remote sensing prediction error presents the largest error term. This error term increases with biomass level, mostly due to saturation of the signal at high biomass. Future work will examine the better characterisation of the other sources of error, and how the spatially distributed per-pixel error propagates to aggregated scales.

4.3. Comparison with previous studies

The amount and spatial distribution of *AGBC* in Mexico differs between published studies (Figs. 13 & 14). Trend analysis of the three-dimensional distribution of *AGBC* was performed over the latitudinal (north–south) and longitudinal (east–west) gradients. There are considerably different spatial trends in the southern-central part of the country, where the TCM-1 and TCM-2 maps display significantly higher amounts of *AGBC* in comparison to the *in-situ* data, MRF, and the AGB-MEX map. The MRF map and AGB-MEX map show similar spatial patterns in the distribution of *AGBC* as well as the overall amount of *AGBC* stocks (Fig. 13). However, the AGB-MEX map characterises the increasing trend in *AGBC* from the dry tropical forests in the northwest of the Yucatan peninsula towards the humid tropical forests of the southeast much more realistically.

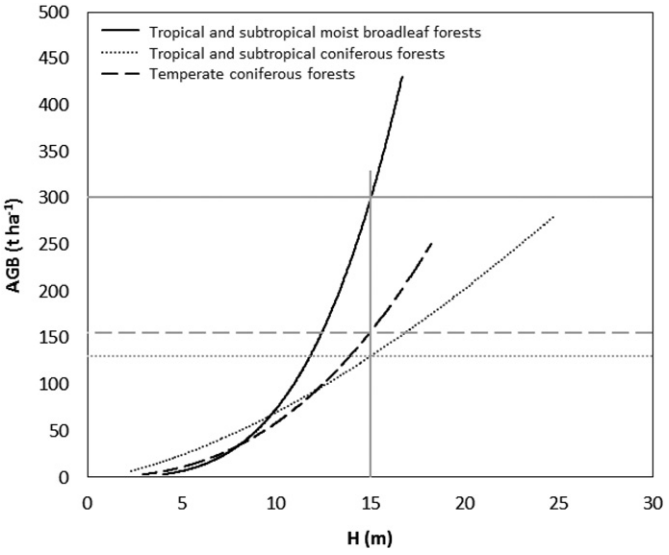

Fig. 15. Plot level *AGB-H* allometry for three different forest biomes in Mexico. *AGB* as a function of mean canopy height of 15 m is marked with horizontal lines. Allometric models were developed using INFyS plot inventory data.

Moran's I tests at state scale were performed (see Table A2 in Appendix A) using the locations of the inventory field plots to assess the different degree of spatial clustering in each map per state. Small states in the centre of the country such as Morelos and Aguascalientes have larger differences between map products. The analysis also shows that the state of Yucatan has much lower spatial clustering in TCM-1 than in any other *AGB* map, which is also seen in Fig. 14. The states of the Yucatan peninsula (Yucatan, Quintana Roo and Campeche) present similar indices for the AGB-MEX and MRF maps.

The total *AGBC* estimated by the AGB-MEX map for 2008 was 1.69 Gt C (21.8 t C ha^{-1}), which is close to the national estimate of 1.68 Gt C reported to FAO (FAO, 2010b), but very different from the TCM-1 and TCM-2 maps (2.24 and 1.95 Gt C respectively). If the LUV mask is used then the estimate was 1.47 Gt C, which is very close to the MRF map estimate (1.53 Gt C). Differences between TCM-1 and TCM-2 have previously been reported (Mitchard et al., 2013). When comparing the pan-tropical maps, the MRF map, the AGB-MEX map and the *in-situ* data, the different temporal coverage might not be sufficient to explain these differences. Even though the spatial modelling approach from TCM-1 is similar to the MaxEnt approach used for the AGB-MEX map, the input data layers differ greatly. All the approaches also face problems relating to the variability of *AGBC* per pixel, due to the difference between the size of the training plots and the pixel area ($\varepsilon_{sampling}$). Using larger sampling plots for training can reduce this uncertainty term in very heterogeneous forest types.

The *AGBC in-situ* data come from a large systematic stratified sampling inventory of the forests in Mexico. It is assumed to be the most representative dataset of the real *AGBC* distribution. In order to compare the *AGBC* estimates from the different maps with the *in-situ* data, the locations of the *in-situ* plots are used to extract the predictions from each map and generate *AGBC* histograms (Fig. 14). The AGB-MEX map shows similar results to the MRF map in terms of spatial distribution and *AGBC* stocks. Both used the INFyS dataset as *AGBC* training data, but here we used MaxEnt to spatially extrapolate the data while MRF used a Random Forest. MRF has a smaller RMSE than AGB-MEX, but the MRF map tends to overestimate small *AGBC* values while high values are underestimated. This is apparent when comparing the histograms of *AGBC*, as MRF has a very narrow distribution in comparison to the INFyS *in-situ* dataset and the AGB-MEX map (Fig. 14). The AGB-MEX histogram represents the variation in the INFyS *in-situ* data much more realistically than any other map examined here.

The two tropical carbon maps (TCM-1 and TCM-2) have similarly high *AGBC* per ha, which exceeds the *AGBC* expected in Mexico according to the INFyS field plots. Dividing the histogram into quantiles shows that 50% of the occurrences for TCM-1 and TCM-2 are above 50 t C ha^{-1}, although the INFyS *in-situ* data suggest no more than 13% (Fig. 14). These differences could be related to the *AGBC* reference data used in those studies. While AGB-MEX and MRF are locally trained using field inventory data, the TCM-1 and TCM-2 are globally trained using *AGBC* estimated from GLAS LiDAR footprints. The Mexican field inventory data are assumed to be the most accurate dataset but they also have limitations. The INFyS database might underestimate *AGBC* for certain forest types as trees with less than 7.5 cm in diameter are not measured. The number of trees not being measured in humid tropical forest might be insignificant in terms of *AGBC*, but this might not be the case for tropical dry forest where trees with diameters below 7.5 cm can account for 26–40% of the total *AGBC* in the plot (Jaramillo, Kauffman, Rentería-Rodríguez, Cummings, & Ellingson, 2003).

The maps using GLAS LiDAR footprints as reference data (TCM-1 and TCM-2) show comparable results to Mitchard et al. (2013), but a different histogram distribution than the INFyS *in-situ* data for the same sampling points (Fig. 14). This is explained by the continental and global approaches used to extrapolate the *AGBC* reference data. The dataset used for extrapolation in TCM-1 covered the whole of Latin America, and therefore the algorithm training was very strongly influenced by the GLAS footprints of the Amazon basin due to their sheer number. Due to the random sampling scheme the footprints can under- or over-represent specific regions and forest types (representativeness of the true distribution of *AGB* accounted for by $\varepsilon_{prediction}$ in this study). The same effect occurs in TCM-2 but at the scale of the entire tropical biome. A single algorithm was used to train the estimation algorithm of *AGBC* which for such a huge area neglects important regional variations in structure and species composition of forest ecosystems.

TCM-1 estimated canopy height using Lefsky's (2010) models and then used three continental-scale allometric models to relate canopy height to *AGB*. The use of a single allometric model for a whole continent might also be the source of discrepancies, as different biomes such as tropical moist forest and temperate coniferous forest have different tree allometries. These allometric differences can also occur at regional scale within the same biome depending on climatic conditions, vegetation structure, species, wood density, soil types and other characteristics (Keith, Barrett, & Keenan, 2000, Chave et al., 2005; Feldpausch et al., 2011), which ultimately affect the relationship between *AGB* and canopy height at plot scale. The slopes of plot-scale allometric relationships between *AGB* and canopy height normally used to calibrate EO data can differ greatly between forest biomes (Fig. 15).

The field inventory plots used in the TCM-1 to develop the continental-scale allometric model for Latin America from the GLAS footprints were mostly located in the Amazon forest region. The use of that model to estimate *AGB* from the GLAS footprints covering Mexico introduces a high uncertainty to the *AGB* estimation ($\varepsilon_{allometry}$), and contributes to the differences shown in Figs. 13 & 14. TCM-2 has the same issue, as *AGB* was estimated from GLAS footprints by a single multiple-regression model for the whole tropical region. The development of regional and biome-specific *AGB-H* models for GLAS footprints and the regionalisation of the algorithm training appears to be the most logical way forward to improve such maps.

5. Conclusions

The current study presents a feasible approach to estimate forest probability, *AGB* and its associated uncertainty using *in-situ* data and a combination of freely available Earth observation datasets. Satellite remote sensing data at 250 m spatial resolution were used to map all forest lands of Mexico. The combination of SAR, optical and elevation datasets (ALOS PALSAR, MODIS, and SRTM) showed better model performance than using a single sensor or combining two sensors. The contribution of each sensor to the *AGB* estimation per biomass range is reported. The carbon stocks of Mexico and its uncertainty are analysed in terms of spatial distribution, forest types, forest masks and biomass ranges. The use of different forest masks can have a large impact on the estimation of national carbon stocks. Even forest masks generated from different sensors using a similar forest definition (*i.e.* from the FAO) present large discrepancies in forest extent and total carbon stocks.

The MaxEnt approach used here is applicable to imagery from sensors that are currently in orbit (MODIS and ALOS-2 PALSAR L-Band SAR) and could also be used with other sensors such as Sentinel-1 C-band, Sentinel-2 and Landsat. The uncertainties found for this approach do not fully meet the requirements articulated for the planned BIOMASS mission (Le Toan et al., 2011; ESA, 2012), but the results suggest that the MaxEnt approach can provide more accurate maps of *AGB* at regional and national scale if larger forest plots at the resolution of the remote sensing imagery were used.

This study also addresses the differences between published forest carbon stock assessments in Mexico. Estimations from tropical carbon maps (TCM-1 and TCM-2) using GLAS LiDAR footprints as training data differ from the *in-situ* forest inventory data (INFyS), and from the maps using this INFyS data as training (AGB-MEX and MRF). Some possible causes are identified and discussed with the error propagation model used here. These differences have implications for national carbon accounting and REDD+. *AGB* reference data are a key component in

explaining the differences, as methods to estimate the spatial distribution of *AGB* are robust and comparable when using the same reference data. Further work has to be done to understand the discrepancies found between *in-situ* data and GLAS LiDAR footprint data.

Conflict of interest

The authors declare no conflict of interest.

Acknowledgments

The authors would like to thank the following people and organizations for providing the data: JAXA (ALOS PALSAR), NASA, GLCF, USGS, and CIAT (MODIS and SRTM), Alessandro Baccini (TCM-2), Oliver Cartus (MRF), INEGI (LUV dataset), and Carlos Edgar Zermeño Benitez and CONAFOR (INFyS dataset). We would also like to thank Andrea Hurtado de Mendoza Rosales (University of Leicester) for providing contacts in Mexico and assistance with the INFyS dataset. The authors would like to also thank the anonymous reviewers for their valuable comments and suggestions to improve the quality of the paper. This work was supported by Copernicus Initial Operations — Network for Earth Observation Research Training (GIONET). GIONET was funded by the European Commission, Marie Curie Programme, Initial Training Networks, Grant Agreement number PITN-GA-2010-264509. P. Rodriguez-Veiga and H. Balzter were supported by the NERC National Centre for Earth Observation (NCEO). H. Balzter was also supported by the Royal Society Wolfson Research Merit Award, 2011/R3.

Appendix A

Table A1
Carbon stocks and forest cover at state level.

State	Total *AGBC* (million t)	Average *AGBC* (t C ha^{-1})	Forest cover (M ha)
Aguascalientes	1.2	10.1	0.12
Baja California	0.5	15.2	0.03
Baja California Sur	2.9	13.7	0.21
Campeche	175.9	38.9	4.52
Chiapas	146.1	25.6	5.71
Chihuahua	103.5	18.3	5.67
Coahuila	21.8	17.8	1.22
Colima	6.5	17.1	0.38
Distrito Federal	3.0	35.7	0.08
Durango	123.8	21.6	5.73
Guanajuato	12.2	12.8	0.95
Guerrero	93.9	16.9	5.55
Hidalgo	24.4	21.1	1.16
Jalisco	75.9	16.6	4.57
México	40.7	25.9	1.57
Michoacán	83.7	18.9	4.42
Morelos	3.7	11.8	0.31
Nayarit	32.9	16.7	1.97
Nuevo León	22.7	22.4	1.01
Oaxaca	176.9	24.4	7.26
Puebla	30.2	14.7	2.05
Querétaro	11.2	19.3	0.58
Quintana Roo	153.8	39.0	3.95
San Luis Potosí	30.4	19.8	1.54
Sinaloa	41.9	15.3	2.74
Sonora	42.2	11.7	3.60
Tabasco	14.7	17.8	0.83
Tamaulipas	46.1	22.0	2.09
Tlaxcala	4.5	18.5	0.24
Veracruz	49.6	18.6	2.66
Yucatán	90.7	29.8	3.04
Zacatecas	20.4	14.1	1.45

Table A2
Moran's I Index within state by *AGB* map. The locations of the inventory plots were used to extract the *AGB* data from each of the carbon maps. The table shows the different degree of spatial clustering of each map per state. All p values <0.001. Note: different size windows were used per state to compute the index (due to the difference in size among states). Therefore, index values are comparable among map products, but not among states.

State	AGB-MEX	MRF	TCM-1	TCM-2
Aguascalientes	0.74	0.52	0.30	0.58
Campeche	0.60	0.59	0.43	0.70
Chiapas	0.40	0.28	0.51	0.45
Colima	0.41	0.37	0.47	0.43
Distrito Federal	0.12	0.10	0.11	0.10
Guanajuato	0.55	0.41	0.18	0.47
Guerrero	0.68	0.52	0.48	0.61
Hidalgo	0.38	0.27	0.42	0.31
Jalisco	0.48	0.35	0.51	0.45
Michoacán	0.40	0.33	0.31	0.36
Morelos	0.82	0.51	0.24	0.50
México	0.51	0.41	0.16	0.32
Nayarit	0.38	0.27	0.44	0.31
Oaxaca	0.57	0.49	0.72	0.69
Puebla	0.43	0.27	0.35	0.43
Querétaro	0.34	0.33	0.32	0.47
Quintana Roo	0.43	0.42	0.26	0.52
Tabasco	0.42	0.30	0.35	0.43
Tlaxcala	0.49	0.41	0.43	0.43
Veracruz	0.54	0.43	0.65	0.52
Yucatán	0.54	0.57	0.28	0.54

References

Asner, G. P., Clark, J. K., Mascaro, J., Galindo García, G. A., Chadwick, K. D., Navarrete Encinales, D. A., ... Ordóñez, M. F. (2012). High-resolution mapping of forest carbon stocks in the Colombian Amazon. *Biogeosciences*, *9*, 2683–2696. http://dx.doi.org/10.5194/BG-9-2683-2012 (ISSN: 1726–4189).

Avitabile, V., Baccini, A., Friedl, M. A., & Schmullius, C. (2012). Capabilities and limitations of landsat and land cover data for aboveground woody biomass estimation of Uganda. *Remote Sensing of Environment*, *117*, 366–380. http://dx.doi.org/10.1016/J.RSE.2011.10.012 (ISSN: 0034–4257).

Baccini, A., Goetz, S. J., Walker, W. S., Laporte, N. T., Sun, M., Sulla-Menashe, D., ... Houghton, R. A. (2012). Estimated carbon dioxide emissions from tropical deforestation improved by carbon-density maps. *Nature clim. Change* Advance online publication, http:/dx.doi.org/http://www.nature.com/nclimate/journal/vaop/ncurrent/abs/nclimate1354.html#supplementary-information. (ISSN: 1758–6798).

Baccini, A., Laporte, N., Goetz, S. J., Sun, M., & Dong, H. (2008). A first map of tropical Africa's above-ground biomass derived from satellite imagery. *Environmental Research Letters*, *3*. http://dx.doi.org/10.1088/1748-9326/3/4/045011 (ISSN: 1748–9326).

Blackard, J. A., Finco, M. V., Helmer, E. H., Holden, G. R., Hoppus, M. L., Jacobs, D. M., ... Tymcio, R. P. (2008). Mapping U.S. forest biomass using nationwide forest inventory data and moderate resolution information. *Remote Sensing of Environment*, *112*, 1658–1677. http://dx.doi.org/10.1016/J.RSE.2007.08.021 (ISSN: 0034–4257).

Breiman, L. (2001). Random Forests. *Machine Learning*, *45*, 5–32 (ISSN: 0885–6125).

Brown, S. (1997). Estimating biomass and biomass change of tropical forests: A primer. *Food & Agriculture Organization (FAO)* (ISBN/ISSN: 9251039550).

Canisius, F., & Fernandes, R. (2012). ALOS PALSAR L-band polarimetric SAR data and in situ measurements for leaf area index assessment. *Remote Sensing Letters*, *3*, 221–229 (ISSN: 2150-704X).

Carreiras, J., Melo, J., & Vasconcelos, M. (2013). Estimating the above-ground biomass in Miombo Savanna woodlands (Mozambique, East Africa) using L-band synthetic aperture radar data. *Remote Sensing*, *5*, 1524–1548 (ISSN: 2072–4292).

Cartus, O., Kellndorfer, J., Walker, W., Franco, C., Bishop, J., Santos, L., & Fuentes, J. (2014). A national detailed map of forest aboveground carbon stocks in Mexico. *Remote Sensing*, *6*, 5559–5588 (ISSN: 2072–4292).

Chave, J., Andalo, C., Brown, S., Cairns, M., Chambers, J., Eamus, D., ... Yamakura, T. (2005). Tree allometry and improved estimation of carbon stocks and balance in tropical forests. *Oecologia*, *145*, 87–99. http://dx.doi.org/10.1007/S00442-005-0100-X (ISSN: 0029–8549).

Chave, J., Condit, R., Aguilar, S., Hernandez, A., Lao, S., & Perez, R. (2004). Error propagation and scaling for tropical forest biomass estimates. *Philosophical Transactions of the Royal Society of London. Series B: Biological sciences*, *359*, 409–420 (ISSN: 0962–8436).

Chave, J., Condit, R., Lao, S., Caspersen, J. P., Foster, R. B., & Hubbell, S. P. (2003). Spatial and temporal variation of biomass in a tropical forest: Results from a large census plot in Panama. *Journal of Ecology*, *91*, 240–252 (ISSN: 1365–2745).

CONAFOR (2012a). Alomexico — modelos alometricos de mexico. ([Online] Available:) http://www.mrv.mx/index.php/en/mrv-m-3/work-areas/allometric-modells

CONAFOR (2012b). *Forest above-ground biomass stocks in Mexico for 2004–2012. Comision Nacional Forestal.*

Dabrowska-Zielinska, K., Budzynska, M., Tomaszewska, M., Bartold, M., Gatkowska, M., Malek, I., ... Napiorkowska, M. (2014). Monitoring wetlands ecosystems using ALOS

PALSAR (L-band, HV) supplemented by optical data: A case study of Biebrza wetlands in Northeast Poland. *Remote Sensing*, *6*, 1605–1633.

Dimiceli, C. M., Carroll, M. L., Sohlberg, R. A., Huang, C., Hansen, M. C., & Townshend, J. R. G. (2011). *Annual global automated MODIS vegetation continuous fields (mod44b) at 250 m spatial resolution for 2008, collection 5 percent tree cover*. College Park, Maryland: University of Maryland.

Elith, J., Phillips, S. J., Hastie, T., Dudík, M., Chee, Y. E., & Yates, C. J. (2011). A statistical explanation of maxent for ecologists. *Diversity and Distributions*, *17*, 43–57 (ISSN: 1472–4642).

ESA (2012). *Biomass report for mission selection.* http:/dx.doi.org/ISBN 978-92-9221-422-7 (3 volumes), ISBN/ISSN: SP-1324/1.

FAO (2005). *Global forest resources assessment 2005*. FAO forestry paper. Food and Agriculture Organization of the United Nations.

FAO (2010a). *FRA 2010, Informe Nacional Mexico*. ROME: Departamento Forestal, Organización De Las Naciones Unidas Para La Agricultura Y La Alimentación.

FAO (2010b). *Global forest resources assessment 2010*. FAO forestry paper. Food and Agriculture Organization of the United Nations.

FAO (2012). *FRA 2015 — terms and definitions*. ROME: Food and Agriculture Organization of the United Nations.

Feldpausch, T. R., Banin, L., Phillips, O. L., Baker, T. R., Lewis, S. L., Quesada, C. A., ... Lloyd, J. (2011). Height–diameter allometry of tropical forest. *BIOGEOSCIENCES*, *8*, 1081–1106. http://dx.doi.org/10.5194/BG-8-1081-2011 (ISSN: 1726–4170).

Freeman, E. A., & Moisen, G. G. (2008). A comparison of the performance of threshold criteria for binary classification in terms of predicted prevalence and kappa. *Ecological Modelling*, *217*, 48–58. http://dx.doi.org/10.1016/J.ECOLMODEL.2008.05.015 (ISSN: 0304–3800).

Gesch, D., Oimoen, M., Greenlee, S., Nelson, C., Steuck, M., & Tyler, D. (2002). The national elevation dataset. *Photogrammetric Engineering and Remote Sensing*, *68*, 5–32 (ISSN: 0099–1112).

Gibbs, H. K., Brown, S., Niles, J. O., & Foley, J. A. (2007). Monitoring and estimating tropical forest carbon stocks: Making REDD a reality. *Environmental Research Letters*, *2*, 045023. http://dx.doi.org/10.1088/1748-9326/2/4/045023 (ISSN: 1748–9326).

Hame, T., Kilpi, J., Ahola, H. A., Rauste, Y., Antropov, O., Rautiainen, M., ... Bounpone, S. (2013a). Improved mapping of tropical forests with optical and SAR imagery, part I: Forest cover and accuracy assessment using multi-resolution data. *Selected Topics In Applied Earth Observations and Remote Sensing, Ieee Journal of*, *6*, 74–91. http://dx.doi.org/10.1109/JSTARS.2013.2241019 (ISSN: 1939–1404).

Hame, T., Rauste, Y., Antropov, O., Ahola, H. A., & Kilpi, J. (2013b). Improved mapping of tropical forests with optical and SAR imagery, part II: Above ground biomass estimation. *Selected Topics In Applied Earth Observations and Remote Sensing, Ieee Journal of*, *6*, 92–101. http://dx.doi.org/10.1109/JSTARS.2013.2241020 (ISSN: 1939–1404).

Hansen, M. C., Defries, R. S., Townshend, J. R. G., Carroll, M., Dimiceli, C., & Sohlberg, R. A. (2003). Global percent tree cover at a spatial resolution of 500 meters: First results of the modis vegetation continuous fields algorithm. *Earth Interactions*, *7*, 1–15. http://dx.doi.org/10.1175/1087-3562(2003)007<0001:GPTCAA>2.0.CO;2.

Hansen, M. C., Potapov, P. V., Moore, R., Hancher, M., Turubanova, S. A., Tyukavina, A., ... Townshend, J. R. G. (2013). High-resolution global maps of 21st-century forest cover change. *Science*, *342*, 850–853. http://dx.doi.org/10.1126/SCIENCE.1244693.

Hastie, T., Tibshirani, R., Friedman, J., & Franklin, J. (2005). The elements of statistical learning: Data mining, inference and prediction. *The Mathematical Intelligencer*, *27*, 83–85 (ISSN: 0343–6993).

Hattab, T., Lasram, F. B. R., Albouy, C., Sammari, C., Romdhane, M. S., Cury, P., ... Le Loc'h, F. (2013). *The use of a predictive habitat model and a fuzzy logic approach for marine management and planning.* (Plos one textbar www.plosone.org).

Hill, T. C., Williams, M., Bloom, A. A., Mitchard, E. T., & Ryan, C. M. (2013). Are inventory based and remotely sensed above-ground biomass estimates consistent? *Plos One*, *8*, E74170 (ISSN: 1932–6203).

Houghton, R. A. (2005). Aboveground forest biomass and the global carbon balance. *Global Change Biology*, *11*, 945–958. http://dx.doi.org/10.1111/J.1365-2486.2005.00955.X (ISSN: 1365–2486).

Houghton, R., Hall, F., & Goetz, S. J. (2009). Importance of biomass in the global carbon cycle. *Journal of Geophysical Research: Biogeosciences (2005–2012)*, *114* (ISSN: 2156–2202).

INEGI (2009). *Cartografia uso de suelo y vegetación*. MEXICO: Instituto Nacional De Estadistica Y Geografia.

INEGI (2014a). *Guía para la interpretación de cartografía: uso del suelo y vegetación: escala 1:250, 000 : serie V*. Mexico: Instituto Nacional De Estadística Y Geografía.

INEGI (2014b). *Recusrsos naturales — uso de suelo y vegetación — productos y servicios*. Instituto Nacional De Estadística Y Geografía Available online: http://www.inegi.org.mx/geo/contenidos/recnat/usosuelo/ [Accessed 2014].

IPCC 2003. Definitions and methodological options to inventory emissions from direct human-induced degradation of forests and devegetation of other vegetation types, prepared by the National Greenhouse Gas Inventories Programme. Timo Karjalainen (Finland) and Gary Richards (Australia), Tomas Hernandez (Mexico), Samuel Kainja (Malawi), Gerry Lawson (Uk), Shirong Liu (China), and Steve Prisley (USA) ed.: Iges, Japan.

Jaramillo, J. V., Kauffman, B. J., Rentería-Rodríguez, L., Cummings, L. D., & Ellingson, J. L. (2003). Biomass, carbon, and nitrogen pools in mexican tropical dry forest landscapes. *Ecosystems*, *6*, 609–629. http://dx.doi.org/10.1007/S10021-002-0195-4 (ISSN: 1432–9840).

Jarvis, A., Reuter, H. I., Nelson, A., & Guevara, E. (2008). *Hole-filled seamless SRTM Data v4, International Centre for Tropical Agriculture (CIAT)*.

JAXA (2014). *New Global 50 m-resolution Palsar Mosaic and Forest/non-forest Map (2007–2010) — Version 1.* [Online] Japan Aerospace Exploration Agency, Kyoto & Carbon Initiative Available: http://www.eorc.jaxa.jp/ALOS/ [Accessed 2014].

Keith, H., Barrett, D., & Keenan, R. (2000). Review allometric relationships for estimating woody biomass. *Technical report 5B. National Carbon Accounting System*. Australian Greenhouse Office.

Kovacs, J., Lu, X., Flores-Verdugo, F., Zhang, C., De Santiago, F. F., & Jiao, X. (2013). Applications of ALOS PALSAR for monitoring biophysical parameters of a degraded black mangrove (*Avicennia germinans*) forest. *Isprs Journal of Photogrammetry and Remote Sensing*, *82*, 102–111 (ISSN: 0924–2716).

Le Toan, T., Quegan, S., Davidson, M. W. J., Balzter, H., Paillou, P., Papathanassiou, K., ... Ulander, L. (2011). The biomass mission: Mapping global forest biomass to better understand the terrestrial carbon cycle. *Remote Sensing of Environment*, *115*, 2850–2860. http://dx.doi.org/10.1016/J.RSE.2011.03.020 (ISSN: 00344257).

Le Toan, T., Quegan, S., Woodward, I., Lomas, M., Delbart, N., & Picard, G. (2004). Relating radar remote sensing of biomass to modelling of forest carbon budgets. *Climatic Change*, *67*, 379–402.

Lefsky, M. A. (2010). A global forest canopy height map from the moderate resolution imaging spectroradiometer and the geoscience laser altimeter system. *Geophysical Research Letters*, *37*, L15401. http://dx.doi.org/10.1029/2010GL043622 (ISSN: 0094–8276).

Li, W., & Guo, Q. (2010). A maximum entropy approach to one-class classification of remote sensing imagery. *International Journal of Remote Sensing*, *31*, 2227–2235. http://dx.doi.org/10.1080/01431161003702245 (ISSN: 0143–1161).

Mitchard, E. T. A., Feldpausch, T. R., Brienen, R. J. W., Lopez-Gonzalez, G., Monteagudo, A., Baker, T. R., ... Phillips, O. L. (2014). Markedly divergent estimates of Amazon forest carbon density from ground plots and satellites. *Global Ecology and Biogeography*, *23*, 935–946. http://dx.doi.org/10.1111/GEB.12168 (ISSN: 1466–8238).

Mitchard, E., Saatchi, S., Baccini, A., Asner, G., Goetz, S., Harris, N., & Brown, S. (2013). Uncertainty in the spatial distribution of tropical forest biomass: A comparison of pan-tropical maps. *Carbon Balance and Management*, *8*(10) (ISSN: 1750–0680).

Mitchard, E. T. A., Saatchi, S. S., Lewis, S. L., Feldpausch, T. R., Woodhouse, I. H., Sonké, B., ... Meir, P. (2011). Measuring biomass changes due to woody encroachment and deforestation/degradation in a forest–savanna boundary region of Central Africa using multi-temporal L-band radar backscatter. *Remote Sensing of Environment*, *115*, 2861–2873. http://dx.doi.org/10.1016/J.RSE.2010.02.022 (ISSN: 0034–4257).

Mitchard, E. T. A., Saatchi, S. S., Woodhouse, I. H., Nangendo, G., Ribeiro, N. S., Williams, M., ... Meir, P. (2009). Using satellite radar backscatter to predict above-ground woody biomass: A consistent relationship across four different african landscapes. *Geophysical Research Letters*, *36*, L23401. http://dx.doi.org/10.1029/2009GL040692 (ISSN: 0094–8276).

Mittermeier, R. A. (1997). *Megadiversity: Earth's biologically wealthiest nations*. Agrupacion Sierra Madre (ISBN: 9686397507).

Montesano, P. M., Nelson, R. F., Dubayah, R. O., Sun, G., Cook, B. D., Ranson, K. J. R., ... Kharuk, V. (2014). The uncertainty of biomass estimates from LIDAR and SAR across a boreal forest structure gradient. *Remote Sensing of Environment*, *154*, 398–407. http://dx.doi.org/10.1016/J.RSE.2014.01.027 (ISSN: 0034–4257).

Montesano, P. M., Nelson, R., Sun, G., Margolis, H., Kerber, A., & Ranson, K. J. (2009). MODIS tree cover validation for the circumpolar taiga–tundra transition zone. *Remote Sensing of Environment*, *113*, 2130–2141. http://dx.doi.org/10.1016/J.RSE.2009.05.021 (ISSN: 0034–4257).

NASA (2008). Modis vegetation indices (VI) 16-day l3 global 250 m (mod13q1). In NASA (Ed.), *Land processes distributed active archive center (LP DAAC)* (5th ed.). Sioux Falls, South Dakota: USGS/Earth Resources Observation And Science (EROS) Center,.

Patenaude, G., Milne, R., & Dawson, T. P. (2005). Synthesis of remote sensing approaches for forest carbon estimation: Reporting to the Kyoto Protocol. *Environmental Science & Policy*, *8*, 161–178. http://dx.doi.org/10.1016/J.ENVSCI.2004.12.010 (ISSN: 1462–9011).

Pearson, R. G., Dawson, T. P., Berry, P. M., & Harrison, P. A. (2002). Species: A spatial evaluation of climate impact on the envelope of species. *Ecological Modelling*, *154*, 289–300. http://dx.doi.org/10.1016/S0304-3800(02)00056-X (ISSN: 0304–3800).

Pearson, R. G., Dawson, T. P., & Liu, C. (2004). Modelling species distributions in britain: A hierarchical integration of climate and land-cover data. *Ecography*, *27*, 285–298. http://dx.doi.org/10.1111/J.0906-7590.2004.03740.X (ISSN: 1600–0587).

Peters-Stanley, M., Hamilton, K., & Yin, D. (2012). *Leveraging the landscape: State of the forest carbon markets 2012*. Washington, DC, USA: Forest Trends' Ecosystem Marketplace.

Phillips, S. J., Anderson, R. P., & Schapire, R. E. (2006). Maximum entropy modeling of species geographic distributions. *Ecological Modelling*, *190*, 231–259. http://dx.doi.org/10.1016/J.ECOLMODEL.2005.03.026 (ISSN: 0304–3800).

Phillips, S. J., Dud, M., & SCHAPIRE, R. E. (2004). A maximum entropy approach to species distribution modeling. *Proceedings of the Twenty-first International Conference on Machine Learning*. BANFF, ALBERTA, CANADA: ACM. http://dx.doi.org/10.1145/1015330.1015412.

Roy, D. P., Ju, J., Kline, K., Scaramuzza, P. L., Kovalskyy, V., Hansen, M., ... Zhang, C. (2010). Web-enabled landsat data (WELD): Landsat ETM+ composited mosaics of the conterminous United States. *Remote Sensing of Environment*, *114*, 35–49. http://dx.doi.org/10.1016/J.RSE.2009.08.011 (ISSN: 0034–4257).

Saatchi, S. S., Harris, N. L., Brown, S., Lefsky, M., Mitchard, E. T. A., Salas, W., ... Morel, A. (2011b). Benchmark map of forest carbon stocks in tropical regions across three continents. *Proceedings of the National Academy Of Sciences*, *108*, 9899–9904. http://dx.doi.org/10.1073/PNAS.1019576108.

Saatchi, S., Marlier, M., Chazdon, R. L., Clark, D. B., & Russell, A. E. (2011a). Impact of spatial variability of tropical forest structure on radar estimation of aboveground biomass. *Remote Sensing of Environment*, *115*, 2836–2849. http://dx.doi.org/10.1016/J.RSE.2010.07.015 (ISSN: 0034–4257).

Santoro, M., Beer, C., Cartus, O., Schmullius, C., Shvidenko, A., Mccallum, I., ... Wiesmann, A. (2011). Retrieval of growing stock volume in boreal forest using hyper-temporal series of Envisat ASAR ScanSAR backscatter measurements. *Remote Sensing of Environment*, *115*, 490–507. http://dx.doi.org/10.1016/J.RSE.2010.09.018 (ISSN: 00344257).

Semarnat, C., & INEGI, INE, INIFAP (2004). *Documento estratégico rector del inventario nacional forestal y de suelos.*

Sexton, J. O., Noojipady, P., Song, X. -P., Feng, M., Song, D. -X., Kim, D. -H., ... Townshend, J. R. (2015). Conservation policy and the measurement of forests. *Nature clim. Change*. http://dx.doi.org/10.1038/NCLIMATE2816 (Advance online publication http://www.nature.com/nclimate/journal/vaop/ncurrent/abs/nclimate2816.html#supplementary-information, ISSN: 1758–6798.).

Sexton, J. O., Song, X. -P., Feng, M., Noojipady, P., Anand, A., Huang, C., ... Dimiceli, C. (2013). Global, 30-m resolution continuous fields of tree cover: Landsat-based rescaling of modis vegetation continuous fields with Lidar-based estimates of error. *International Journal of Digital Earth*, *6*, 427–448 (ISSN: 1753–8947).

Shimada, M., & Isoguchi, O. (2002). JERS-1 SAR mosaics of Southeast Asia using calibrated path images. *International Journal of Remote Sensing*, *23*, 1507–1526 (ISSN: 0143–1161).

Shimada, M., Isoguchi, O., Motooka, T., Shiraishi, T., Mukaida, A., Okumura, H., ... Itoh, T. (2011 JULY 24–29). Generation of 10 m resolution PALSAR and JERS-SAR mosaic and forest/non-forest maps for forest carbon tracking. *Geoscience and Remote Sensing Symposium (Igarss), 2011 Ieee International*, 3510–3513 2011.

Shimada, M., Itoh, T., Motooka, T., Watanabe, M., Shiraishi, T., Thapa, R., & Lucas, R. (2014). New global forest/non-forest maps from ALOS PALSAR data (2007–2010). *Remote Sensing of Environment*, *155*, 13–31. http://dx.doi.org/10.1016/J.RSE.2014.04.014 (ISSN: 0034–4257).

Simard, M., Pinto, N., Fisher, J. B., & Baccini, A. (2011). Mapping forest canopy height globally with spaceborne lidar. *Journal of Geophysical Research*, *116*, G04021. http://dx.doi.org/10.1029/2011JG001708.

Thiel, C. J., Thiel, C., & Schmullius, C. C. (2009). Operational large-area forest monitoring in siberia using ALOS PALSAR summer intensities and winter coherence. *Geoscience and Remote Sensing, Ieee Transactions On*, *47*, 3993–4000 (ISSN: 0196–2892).

Thurner, M., Beer, C., Santoro, M., Carvalhais, N., Wutzler, T., Schepaschenko, D., ... Schmullius, C. (2014). Carbon stock and density of northern boreal and temperate forests. *Global Ecology and Biogeography*, *23*, 297–310. http://dx.doi.org/10.1111/GEB.12125 (ISSN: 1466–8238).

usgs (2006). *Shuttle radar topography mission, 3 arc second* (2.0 ed.). College Park, Maryland: Global Land Cover Facility, University Of Maryland.

USGS (2012). MODIS vegetation indices (VI) 16-day products (mod13q1). [online]. Available http://e4ftl01.cr.usgs.gov/MOLT/MOD13Q1.005/ [Accessed 2012]

Vogelmann, J. E., Howard, S. M., Yang, L., Larson, C. R., Wylie, B. K., & Van Driel, N. (2001). Completion of the 1990s national land cover data set for the conterminous United States from landsat thematic mapper data and ancillary data sources. *Photogrammetric Engineering and Remote Sensing*, *67* (ISSN: 0099–1112).

Wadsworth, R., Balzter, H., Gerard, F., George, C., Comber, A., & Fisher, P. (2008). An environmental assessment of land cover and land use change in Central Siberia using quantified conceptual overlaps to reconcile inconsistent data sets. *Journal of Land Use Science*, *3*, 251–264. http://dx.doi.org/10.1080/17474230802559629 (ISSN: 1747-423X).

Wagner, W., Luckman, A., Vietmeier, J., Tansey, K., Balzter, H., Schmullius, C., ... Yu, J. J. (2003). Large-scale mapping of boreal forest in Siberia using ERS tandem coherence and JERS backscatter data. *Remote Sensing of Environment*, *85*, 125–144. http://dx.doi.org/10.1016/S0034-4257(02)00198–0 (ISSN: 0034–4257).

Wollan, A. K., Bakkestuen, V., Kauserud, H., Gulden, G., & Halvorsen, R. (2008). Modelling and predicting fungal distribution patterns using herbarium data. *Journal of Biogeography*, *35*, 2298–2310. http://dx.doi.org/10.1111/J.1365-2699.2008.01965.X (ISSN: 1365–2699).